Technical Report

TR-12-06

Fundamental aspects of stress corrosion cracking of copper relevant to the Swedish deep geologic repository concept

Ganesh Bhaskaran, Anatolie Carcea, Jagan Ulaganathan, Shengchun Wang, Yin Huang, Roger C Newman

Department of Chemical Engineering and Applied Chemistry, University of Toronto

March 2013

Svensk Kärnbränslehantering AB
Swedish Nuclear Fuel
and Waste Management Co

Box 250, SE-101 24 Stockholm
Phone +46 8 459 84 00

SKB

ISSN 1404-0344
SKB TR-12-06
ID 1314566

Fundamental aspects of stress corrosion cracking of copper relevant to the Swedish deep geologic repository concept

Ganesh Bhaskaran, Anatolie Carcea, Jagan Ulaganathan,
Shengchun Wang, Yin Huang, Roger C Newman
Department of Chemical Engineering and Applied Chemistry,
University of Toronto

March 2013

Summary

Phosphorus-doped oxygen-free copper will be used as the outer barrier in canisters that will contain spent nuclear fuel in the proposed Swedish underground repository. The possibility of stress corrosion cracking (SCC) is a concern, in view of isolated reports of cracking or intergranular corrosion of pure copper in sulfide solutions. This concern was addressed in the present work using copper tensile specimens provided by SKB. Methods included slow strain rate testing, constant strain tensile testing, electrochemical and surface analytical studies of corrosion products, and electron backscatter diffraction analysis of grain orientation effects on corrosion. The base solutions were prepared from NaCl or synthetic sea water with addition of varying amounts of sodium sulfide at room temperature and 80°C.

No SCC was found in any of the testing, for a range of sulfide concentrations from 5–50 mM at room temperature or 80°C, including tests where small anodic or cathodic potential displacements were applied from the open-circuit (corrosion) potential. Neither was SCC found in constant-strain immersion testing with very large strain.

The Cu_2S corrosion product is generally very coarse, fragile, and easily spalled off in severe corrosion environments, i.e. high sulfide concentration, high temperature, less perfect deaeration, etc. But it could also consist of very fine grains, relatively compact and adherent, on particular grain orientations when it was formed on an electropolished surface in a very well-deaerated solution. These orientations have not yet been identified statistically, although some preference for thin, adherent films was noted on orientations close to (100). The notion that the corrosion reaction is always controlled by inward aqueous-phase diffusion of sulfide may thus not be unconditionally correct for this range of sulfide concentrations; however it is hard to distinguish the role of diffusion within pores in the film. In the actual repository, the limiting flux of sulfide to the canister surface will be some orders of magnitude lower, in view of the bentonite barrier which imposes a lower diffusivity and much longer diffusion length. Preferential corrosion along grain boundaries was rarely observed, which is considered to be important for SCC resistance since there was usually a fairly rapid general corrosion, at least on one side of the grain boundary. Severe plastic deformation was not found to cause any particular localization of corrosion, but may promote general corrosion in the deformed area. On the basis of this work, SCC of copper in sulfide solution, obtained by Japanese workers using slow strain rate testing of copper sheet, appears not to be reproducible in the SKB copper using normal tensile specimens. Neither can we rationalize, on the basis of our results, the findings of Finnish workers on intergranular corrosion emanating from a fatigue crack tip. Some complexities related to these other studies are discussed, including the possible effect of poor deaeration or inappropriate potential control; however a discrepancy remains nonetheless.

Contents

1 Introduction

The possibility of stress corrosion cracking (SCC) of copper in aqueous sulfide solutions was introduced by Taniguchi and Kawasaki (2008). These authors used flat slow-strain-rate (SSR) tensile specimens and a testing solution made from artificial seawater with Na_2S added. This is actually a complex mixture, because Na_2S is a base (dissociating completely into Na^+ and HS^-, and liberating an equivalent amount of OH^-, when dissolved in water[1]), while artificial seawater contains substances that consume OH^- (Ca^{2+}/HCO_3^- and possibly Mg^{2+}). So, while a 10 mM solution of Na_2S has a pH of about 12, the same amount of Na_2S added to artificial seawater gives a pH of only about 9–10, and calcium carbonate is precipitated. The final pH will depend on the sulfide concentration. But despite these complexities, clear evidence of intergranular SCC was observed in a solution containing 10 mM sulfide at 80°C.

There are some questions about the replenishment of the solution in the work of Taniguchi and Kawasaki, at least for immersion testing – the SCC tests appear to have been refreshed. Also, they adopted an unusual procedure in which the tensile specimen was first allowed to stabilize at its open-circuit potential (OCP) for an unstated time, then the potential was controlled thereafter at this fixed value. If there is a long-term drift of the natural OCP, then the outcome of such a procedure will be a small cathodic or anodic polarization of the specimen from its OCP. We do not understand why such a procedure was necessary – we can only speculate that there were other metals in the system which, if they became exposed during a test (e.g. by failure of a coating), would have caused a galvanic effect were it not for the potentiostatic polarization.

It was recognized early on in this project that if no SCC was obtained during simple SSR testing under the conditions of Taniguchi and Kawasaki, there would be a range of parameters that would need to be explored to decide whether their result was reproducible or not.

More recently, we have been informed about a study carried out in Finland in which deep intergranular corrosion or cracking was observed ahead of fatigue cracks in precracked copper CT specimens exposed to sulfide-containing solutions with 10 or 100 ppm of sulfide (Arilahti et al. 2011a, b). There can be little doubt that deep intergranular corrosion or SCC, extending for millimeters ahead of the fatigue crack tip over a period of some weeks, occurred in this work. The authors claim that this was due to 'diffusion of sulfur or sulfide ahead of the crack', but if this is envisaged as a solid-state process, it would be unprecedented; a more normal interpretation would be that the aqueous solution is always present at the crack tip within the nanoscale pores of a Cu_2S or similar film. Many SCC processes show cracks apparently filled with corrosion product, yet there is water at the crack tip. As with the work of Taniguchi and Kawasaki, there are some questions as to the potential seen by the specimens, which seems to have been more positive than the reversible hydrogen electrode potential for the applicable pH, suggesting that oxidizing impurities were present.

The electrochemistry of corrosion of copper in sulfide solutions was studied by Smith et al. (2007) and by Smith in his thesis (Smith 2007). Sulfidation to Cu_2S occurs below the reversible hydrogen electrode potential, so corrosion and (in principle) SCC are certainly possible in practice. The surface films tended to be quite unprotective; the corresponding transport mechanisms, whether solution-phase, interfacial or solid-state, have not been fully worked out to our knowledge. A particularly significant possibility, for the nuclear waste problem, is that even at quite high sulfide concentrations, the corrosion rate tends to be controlled by inward diffusion of sulfide, through the solution boundary layer and/or the pores in the sulfide film. If this were to be the case in a repository (where the sulfide concentration is lower and the diffusion length much longer, and the diffusion coefficient much smaller, than in published laboratory studies), it should be physically impossible for localized

[1] The idea that S^{2-} is stable under such conditions is due to the adoption of faulty chemical potential data in the Pourbaix 'Atlas'. For a recent discussion of this point, see Sun et al. (2008).

corrosion or SCC to be sustained, provided that the width of the slot, crack or pit – however one models the corrosion geometry – is much less than the diffusion layer thickness[2].

It is not a trivial matter to determine whether or not corrosion is controlled by inward aqueous-phase sulfide diffusion through a corrosion product layer, because the usual methods for doing that involve varying the potential, and there is not much of a potential window within which that can be done without perturbing the processes occurring; capacitive currents may also interfere. One could try to gain information from electrochemical impedance studies, or by making step changes in sulfide concentration, but it is unlikely those results will be conclusive one way or the other. A hydrodynamically modulated rotating disk electrode may, in principle, be able to separate pore diffusion from boundary layer diffusion.

An aspect of the copper-sulfide corrosion problem that has caused a certain confusion is the existence of soluble sulfide complexes of Cu(I). Smith mentioned dissolution-reprecipitation as a possible mechanism of the formation of porous Cu_2S films, and such a mechanism naturally produces abrupt transitions between protective and non-protective film formation with parameters such as sulfide concentration and precorrosion, as shown by Newman et al. (1992) for iron. While preparing this report, we were surprised to find how well-known such complexes were in some communities, and their properties have even been calculated using *ab initio* quantum chemistry (Tossell 2000). The log of the stability constant for the complex $Cu(SH)_2^-$ is 17.2 according to standard literature. Using other data from the Pourbaix *Atlas* (not current, but good enough for present purposes), we obtain a standard electrode potential of –0.51 V for the equilibrium:

$$Cu(SH)_2^- + e^- = Cu + 2HS^-$$

And the following Nernst equation at 298K:

$$E = -0.51 - 0.118 \log (HS^-) + 0.059 \log (Cu(SH)_2^-) \text{ volts}$$

This is undoubtedly a simplification, as can be seen from the elaborate review given by Rickard and Luther (2006). Some authors even blur the distinction between ‘complexes’ and ‘nanoparticles’. But anyway, using the –0.51 V figure for E^0, and given the corrosion potential values of ca –0.90 V SCE (–0.66 V SHE) shown later on, it is obvious that dissolution as $Cu(SH)_2^-$ is a feasible parallel reaction to Cu_2S formation, but only at high sulfide concentrations; by the time we get down to 1 mM sulfide, the steep 118 mV slope has displaced the dissolution equilibrium to a much higher potential than those observed. Further investigation may show that the neutral complex $Cu(SH)^0$ is more likely to play a role at lower sulfide concentrations, and indeed it is hard to believe that there is no dissolution of copper involved in Cu_2S film formation – the behaviour is so similar to that of iron. One might appeal to Cu(I) chloro complexes when chloride is present, but while chloride does affect the corrosion kinetics, qualitatively similar sulfide films do form without chloride.

[2] This is obviously true for the case where the environment both inside and outside the corrosion site can be modelled as a simple convecting aqueous solution. Sulfide diffusion control of the corrosion rate fixes the limiting sulfide flux and sets the sulfide concentration at the metal surface to zero; any cavity much narrower than the diffusion layer thickness must have a lower sulfide flux, and thus a lower corrosion rate than the general surface. It is not as simple as that for the case where the dominant diffusion barrier is a microporous surface corrosion product, especially when that has a spatially variable sulfide permeability, and more work on that problem would be beneficial. In a non-convecting system with a clay overpack, where the surface corrosion product might never become protective enough to dominate the diffusion problem, the criteria should be similar to those for an aqueous solution, with the added benefit of a much lower limiting sulfide flux.

2 Experimental

The corrosion and cracking behavior of phosphorus doped copper and oxygen free high conductivity (OFHC) pure copper in sodium chloride solution and synthetic sea water with additions of sodium sulfide was studied as follows.

2.1 Slow strain rate testing (SSRT)

SSRT tensile specimens as shown in Figure 2-1 were made. The material was phosphorus doped copper which was provided by SKB (the first batch was obtained through the University of Western Ontario). Specimens were taken from the lid center, the lid edge or the container wall as identified later in the results section. Slow strain rate tests were run on a CERT (constant extension rate test) platform made by Cortest Inc. at strain rates of 10^{-6} or 10^{-7} s^{-1}. Unless otherwise specified, each copper SSRT specimen was preloaded to about 320 kgf before testing, both to save time and to pass over the misleading initial (elastic) part of the stress-strain curve, when much of the elongation is taking up the compliance of the testing machine. The gauge length part of each tensile specimen was etched for 2–3 minutes at 1.2 V after electropolishing in 57 wt.% phosphoric acid for 5–10 minutes at 1.8 V versus a copper cathode. In some tests, that part of the surface was just abraded with silicon carbide paper to a 1200 grit finish.

About 330 mL of either 100 mM NaCl solution (ACS grade NaCl in deionized water) or synthetic sea water, each with addition of the required amount of anhydrous Na_2S, was used in each test. The anhydrous Na_2S was provided by Alfa Aesar. The synthetic seawater was prepared by dissolving 30 g of sea salt (Marine Enterprises) in 1 litre of de-ionized water. The nominal composition of the synthetic sea water is given in Table 2-1. The main reason for using the synthetic seawater, which is otherwise a bothersome environment to work with, was that this was used by Taniguchi and Kawasaki (2008).

After setting up the testing rig with the SSRT sample, NaCl solution or synthetic sea water was filled into the corrosion cell and deaerated for more than 1 hour with high-purity nitrogen. Then the required amount of sodium sulfide was added, and the cell was sealed. For 100 mM sodium chloride, the pH increased to 12 when 10 mM of Na_2S was added. The synthetic seawater had an initial pH of 8.3; when 10 mM Na_2S was added to this solution, the pH increased to about 10, and calcium carbonate was precipitated. In some tests, the pH of the solution was adjusted to near-neutral with concentrated HCl.

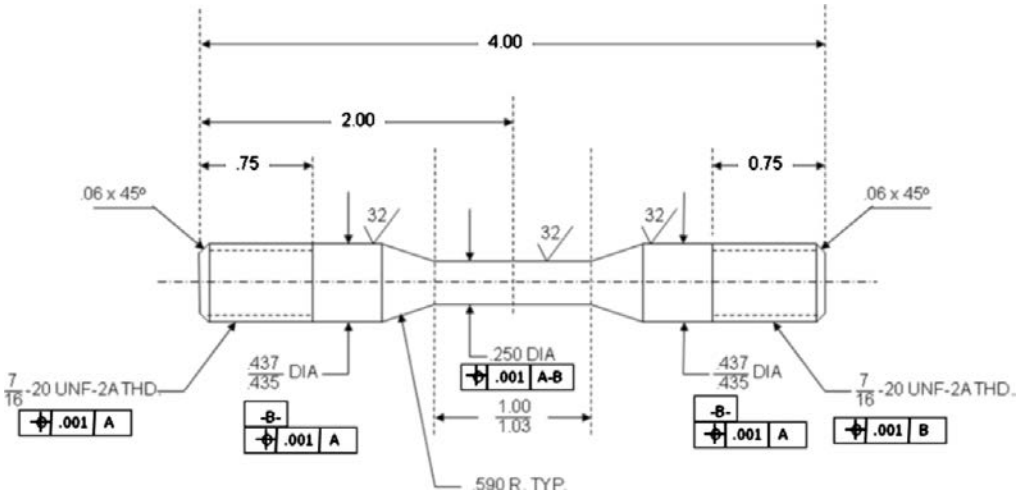

Figure 2-1. *Schematic illustration of the copper SSRT specimen (unit: inch).*

Table 2-1. Nominal composition of the synthetic seawater supplied by the sea salt provider.

Elements	Concentration (mM)	Elements	Concentration (mM)
Cl^-	524	HCO_3^-	2.4
Na^+	452	Sr^{2+}	0.14
SO_4^{2-}	27.1	CO_3^{2-}	0.17
Mg^{2+}	53.7	Br^-	0.075
Ca^{2+}	10.2	BO_3^-	0.075
K^+	9.7	F^-	0.079

The SSRT tests were done at room temperature and 80°C. The test solution was refreshed once in every two days in tests at 80°C, but not in tests at room temperature, where the corrosion rate and thus sulfide consumption rate, was much lower. All tests were done at the open circuit potential unless otherwise mentioned.

In a number of the SSRT tests, straining was interrupted after 3–5% strain at strain rates as low as 10^{-7} s^{-1}. In the other tests, the specimens were strained to failure at a strain rate of 10^{-5}–10^{-6} s^{-1}. After each test, the specimen was immersed in concentrated HCl to remove the sulfide film (with varying degrees of completeness) before surface morphology examination. (In some tests, the sulfide film was removed by immersing in 80% phosphoric acid solution for 20 seconds). Fracture surfaces, side surfaces and longitudinal sections of the gauge part of each tensile specimen were examined.

2.2 Electrochemical behaviour of copper in sulfide solutions

The open circuit potentials (OCP) of the copper from SKB were measured in deaerated 100 mM NaCl solution and in synthetic sea water, each with 10 mM Na_2S additions. The pH of these solutions was not adjusted. Electrochemical impedance spectroscopy (EIS) was also done in these solutions as a function of immersion time. A saturated calomel reference electrode (SCE), platinum wire counter electrode and various software-controlled electrochemical equipment (Gamry Reference 600, Gamry Femtostat, EG&G Parstat 2263) were used. In some initial testing without chloride, a mercury/mercurous sulfate/saturated K_2SO_4 reference electrode (MSE) was used.

Copper sheet of 2 mm thickness and purity 99.99%, provided by Alfa Aesar, was also adopted for electrochemical polarization studies. The copper sheet was cut and mounted in epoxy resin with about 1 cm^2 surface area exposed in each specimen. These specimens were abraded to 1200 grit finish, then electropolished in 57 wt.% phosphoric acid. A saturated calomel reference electrode (SCE) was used.

EIS in the range of 100 kHz–0.1 Hz was applied at ± 10 mV vs. corrosion potential in synthetic seawater with addition of 10 mM Na_2S at room temperature following the procedure in Figure 2-2, to examine the effect of stirring on sulfide film development. Impedance measurements were conducted at points A to F. The specimen was made of SKB copper.

To study the possibility of soluble (or transiently soluble) corrosion products in sulfide-containing solutions, a gold microelectrode probe was adopted. The gauge part of a tensile specimen as shown in Figure 2-1 was cut out and mounted in epoxy resin. One end of the sample was abraded to expose the copper. Then this end was immersed in 70 wt.% HNO_3 for 30 minutes to create a 2.5 mm deep cavity. A small gold disk electrode of 0.25 mm diameter was placed approximately 2 mm from the copper surface of the cavity as shown in Figure 2-3. The whole setup was then placed in a 300 ml beaker containing synthetic seawater. After purging with nitrogen for one hour, 10 mM Na_2S was added to the solution. The gold microelectrode was connected to the working electrode lead of a potentiostat and cyclic voltammetry was carried out. A scan rate of 50 mV/s was used in the potential window of –1.2 to 0.1 V vs. SCE. A separate voltammetry scan was carried out under the same conditions in the absence of the copper sample.

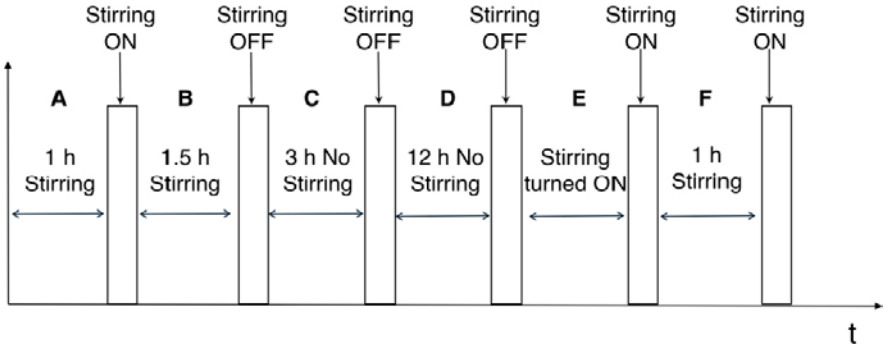

Figure 2-2. *Stirring control in the impedance measurement in synthetic seawater with addition of 10 mM Na_2S at room temperature. The 6 legends at the top indicate the timing and conditions for the impedance measurements shown later (Figure 3-10).*

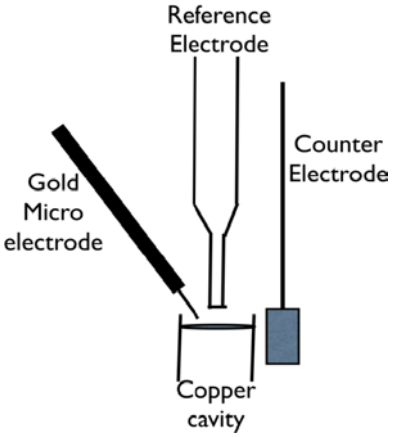

Figure 2-3. *Schematic illustration of the corrosion cell set up with a gold sensor electrode.*

2.3 Constant strain tensile testing

Constant strain tensile tests on tensile specimens as shown in Figure 2-1, U-bend tests, and tests on residually stressed specimens with punch dents were also conducted in several different sulfide-containing solutions at room temperature to check the possibility of SCC. So far as SCC is concerned, these are not of much significance, as nothing interesting was observed. The reason for doing these apparently random-looking tests was to explore some parameter space that was not used in the main investigation, and to use a more rigorous deoxygenation procedure than was possible in the SSRT testing (also deliberately poor deoxygenation in some cases), for subsequent examination of polished flat samples that were immersed along with the strained samples.

For completeness, the conditions examined were as follows:

Tensile specimen as Figure 2-1, as-received finish, 2.4% plastic strain, 10 mM sulfide as H_2S (Ricca Chemicals), no supporting electrolyte, 25°C, 186 hours immersion, with or without deaeration. Also unstrained SKB copper block specimen for comparison.

As above, but electropolished surfaces; 9.2% strain; 259 hours immersion.

U-bend specimen, Goodfellow OFHC copper, 3 mm thick. 10 mM and 100 mM sulfide as Na_2S added to 0.5M NaCl; 162 hours immersion.

Electropolished and then punch-indented specimens (1 mm-dia. spherical punch; SKB copper blocks). Artificial seawater with 2, 10 and 50 mM sulfide as Na_2S. 140 hours immersion. Parallel unpunched samples used for SEM, AES and EBSD studies.

2.4 Auger electron spectroscopy

Auger analyses were carried out at Surface Science Western, University of Western Ontario. The instrument had imaging capability that enabled the sulfide film to be depth-profiled on individual grain surfaces showing sulfide films of different morphology and thickness.

Auger analyses were performed using 10 keV electron beam rastered over a 30×30 micron area. Sputtering was performed using 3 keV Ar+ ion beam rastered over a 1×1 mm area. The sputter rate was determined to be ~20 nm/min for a SiO_2 layer, which would need to be calibrated against Cu_2S in more precise work. The samples were contaminated with carbon from prior SEM examination, but this did not affect the analyses adversely. Approximate film thicknesses could be estimated from prior analyses on analogous samples.

2.5 SEM, EDX and EBSD

A qualitative estimate of sulfide film thickness on grains of varying orientations could be attained by EDX analyses showing apparent 'sulfur concentrations' of several tens of percent down to 1% or even lower – normally, the latter would indicate, for a stoichiometric compound like Cu_2S, a film thickness of order 50 nm, depending on the accelerating voltage.

For EBSD analysis, square samples were cut from the SKB copper block. One face of each sample was ground to a 1200 grit finish followed by polishing to a mirror finish (0.05 microns). The unpolished faces were painted with an insulating lacquer, exposing a polished area of 1 cm^2. Then the samples were electropolished in 57 wt.% phosphoric acid solution for 5 min. A voltage of 2 V was applied with respect to a copper cathode. After electropolishing, the samples were rinsed and washed in de-ionized water and anhydrous methanol. The exposed grain faces were indexed by EBSD using a Hitachi S-4500 field emission electron microscope. A scan step size of 5 microns was used. After indexing the samples were electropolished for 60 s, to remove the deposited carbon on the scanned area. Typically a thickness of 1.5 microns was removed during this secondary electro-polishing. Synthetic seawater was purged with nitrogen, and 2 mM Na_2S solution was added in a glove box. The samples were then placed in 300 ml glass bottles, filled with the above solution and tightly sealed. The samples were exposed for two days in the sulfide polluted synthetic seawater inside the glove box. After exposure, the samples were rinsed in deionized water and anhydrous alcohol. Then the indexed area was examined under the SEM.

3 Results and discussion

3.1 SSRT tests

All the SSRT tests are summarized in Table 3-1. SSRT tests were conducted in 100 mM NaCl solution and in synthetic sea water with additions of 5 mM, 10 mM and sometimes 20 or 50 mM Na_2S at room temperature and 80°C. The gauge length surface of tensile specimens in Test A and Tests 1 to 17 was etched for 2–3 minutes at 1.2 V after it was electropolished in concentrated phosphoric acid for 5–10 minutes at 1.8 V (vs. a copper cathode). Other specimens in Tests B to E and Tests 18 to 25 were just abraded with silicon carbide paper to a 1200 grit finish.

In Tests 1 to 6, the specimen elongation was controlled to be below 5%. This was partly to preserve surface details and partly to avoid applying unrealistic strains – many SCC processes start near the UTS in a SSRT and thus would not occur in real life. However, because there was no SCC found in these tests, specimens were strained to failure in later tests.

Table 3-1. Summary of SSRT tests. RT – Room Temperature, SSW – Synthetic Sea Water, D – Ductile fracture, R – Rough surface with no SCC, N – No SCC.

Test	S^{2-} (mM)	Test solution, T (°C)	pH start to end	Preload (MPa)	Strain rate (s^{-1})	Elongation (%)	UTS (MPa)	Surface features
A	–	Air, RT	–	–	10^{-5}	58 ± 2 (several same tests)	198	D
1	5	100 mM NaCl, RT	12.1 to 10.8	–	10^{-6}	10	NA	R
2	5	100 mM NaCl, RT	12.1 to 11.0	–	10^{-7}	2.2	NA	R
3	5	100 mM NaCl, RT	12.1 to 11.0	–	10^{-7}	2.5	NA	R
4	5	100 mM NaCl, RT	12.1 to 10.8	–	10^{-6}	4.5	NA	R
5	5	100 mM NaCl, RT	12.1 to 11.0	98	10^{-7}	3.2	NA	R
6	10	100 mM NaCl, RT	12.3 to 11.8	98	10^{-7}	2.8	NA	R
7	10	100 mM NaCl, RT	7.5 (adjusted) to 9.8	98	10^{-6}	57.4	177	R
8	5	100 mM NaCl, RT	12.1 to 11.0	98	10^{-6}	56.6	181	R
9	5	100 mM NaCl, RT	7.3 (adjusted) to 9.6	98	10^{-6}	57.6	180	R
10	50	100 mM NaCl, RT	12.3 to 11.0	–	10^{-5}	56.1	178	> 1 mm thick S^{2-} film; stopped and tested in 10 mM sulfide to failure
11	10	100 mM NaCl, RT	12.3 to 11.7	–	10^{-5}	56.2	173	R
12	5	100 mM NaCl, RT	12.1 to 11.6	108	10^{-5}	49.5	167	R (Specimen polished to a cross section diameter of 0.22″ before test)
13	20	100 mM NaCl, RT	12.3 to 11.4	99	10^{-5}	48.2	168	R (Specimen polished to a cross section diameter of 0.22″ before test)
14	10	100 mM NaCl, RT	12.3 to 11.3	98	10^{-5}	35.2	141	R (Specimen polished to a cross section diameter of 0.19″ before test)
15	10	SSW, RT	10.1 to 10.1	98	10^{-5}	Failed due to machine error		R
16	10	SSW, RT	10.1 to 9.5	98	10^{-5}	57.2	176	R
17	10	SSW, 80°C	10.3 to 10.3	98	10^{-6}	50.8	163	R

Test			S^{2-} (mM)	Test solution, T (°C)	pH start to end	Preload (MPa)	Strain rate (s^{-1})	Elongation (%)	UTS (MPa)	Surface features
Cu from SKB Canister lid	Centre	B	–	Air, RT	–	70	10^{-6}	60.2	191	D
	Edge	C	–	Air, RT	–	70	10^{-6}	61.5	195	D
		D	–	Air, RT	–	70	10^{-6}	60.6	192	D
Cu from UWO		E	–	Air, RT	–	70	10^{-6}	58.6	197	D
Cu from SKB Canister lid	Centre	18	5	SSW, RT	10 to 9.4	70	10^{-6}	59.4	189	N
		19	10	SSW, RT	10.1 to 9.5	70	10^{-6}	58.4	187	N
	Edge	20	5	SSW, RT	10 to 9.4	70	10^{-6}	60.0	190	N
		21	10	SSW, RT	10.1 to 9.5	70	10^{-6}	56.8	186	N
		22	10	SSW, RT (–20 mV vs. OCP)	10.1 to 9.01	70	10^{-6}	59.4	187	N
	Centre	23	10	SSW, 80°C	10.1 to 8.7	70	10^{-6}	50.4	162	Severe surface corrosion, no SCC
24			10	SSW, 80°C refreshed each 2 days (–950 mV_{SCE})	10.1 to 9.3	70	10^{-6}	56.9	173	N
25			10	SSW, 80°C refreshed each 2 days (–900 mV_{SCE})	10.1 to 9.3	70	10^{-6}	55.4	171	N
26			10	SSW, 80°C refreshed each 2 days (–800 mV_{SCE})	10.1 to 9.3	70	10^{-6}	53.4	168	N

In some tests, cathodic or anodic polarization was applied during testing, to explore possible artefacts in the procedure of Taniguchi and Kawasaki. As can be seen in Table 3-1, no SCC was found in any test. Typical stress-strain curves obtained are showed in Figure 3-1, which are based on Test C, Test 21 and Test 22, and in Figure 3-2, which are based on Test 24, Test 25 and Test 26. The potentials applied in Test 24, Test 25 and Test 26 were based on the polarization curve as shown in Figure 3-3. There was never any significant difference in elongation between specimens tested in solution and air.

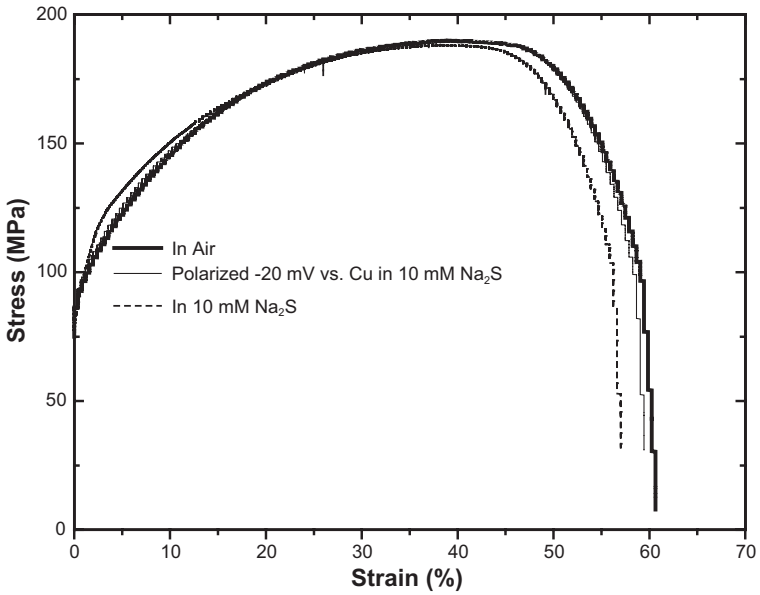

Figure 3-1. *Stress-strain curves obtained from Test C, Test 21 and Test 22 in synthetic seawater with addition of 10 mM Na_2S at room temperature. In test 22, cathodic polarization was applied.*

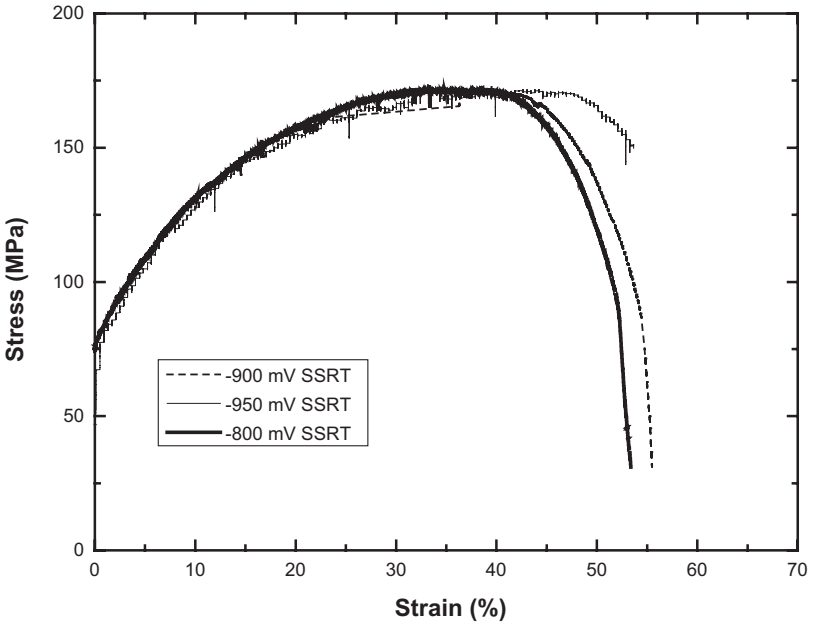

Figure 3-2. *Stress-strain curves obtained from Test 24, Test 25 and Test 26 in synthetic seawater with addition of 10 mM Na_2S at 80°C, undertaken in order to test the possibility that Taniguchi and Kawasaki (2008) obtained SCC because they applied a [unknown] potential.*

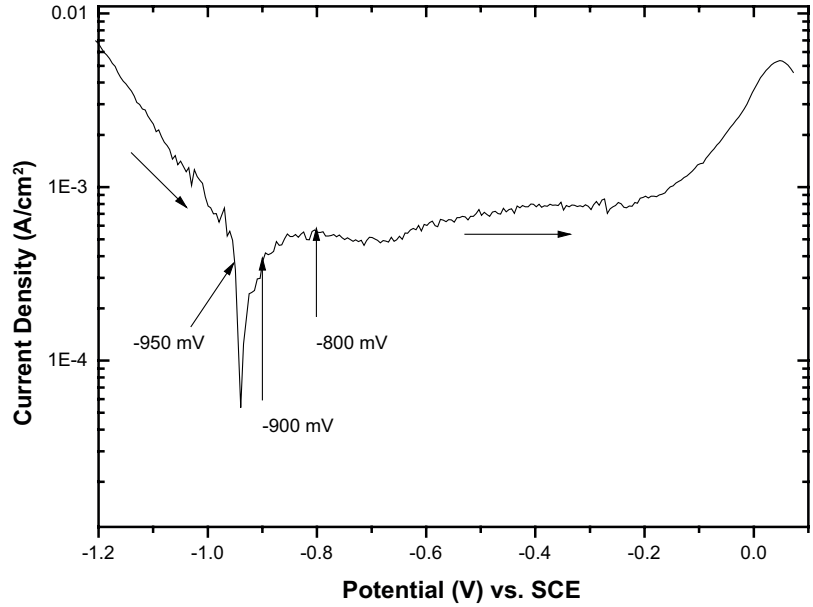

Figure 3-3. *Potentiodynamic scan of copper in synthetic sea water with addition of 10 mM Na_2S at 80°C. Scan rate was 1 mV/s.*

Typical specimen surface morphology after testing is shown in Figure 3-4, which was obtained from Tests 7, 9, 16 and 17 as shown in Table 3-1. A tensile specimen cross section is shown in Figure 3-5, from Test 19 (Table 3-1). It can be seen from these figures that there was general surface corrosion in every test.

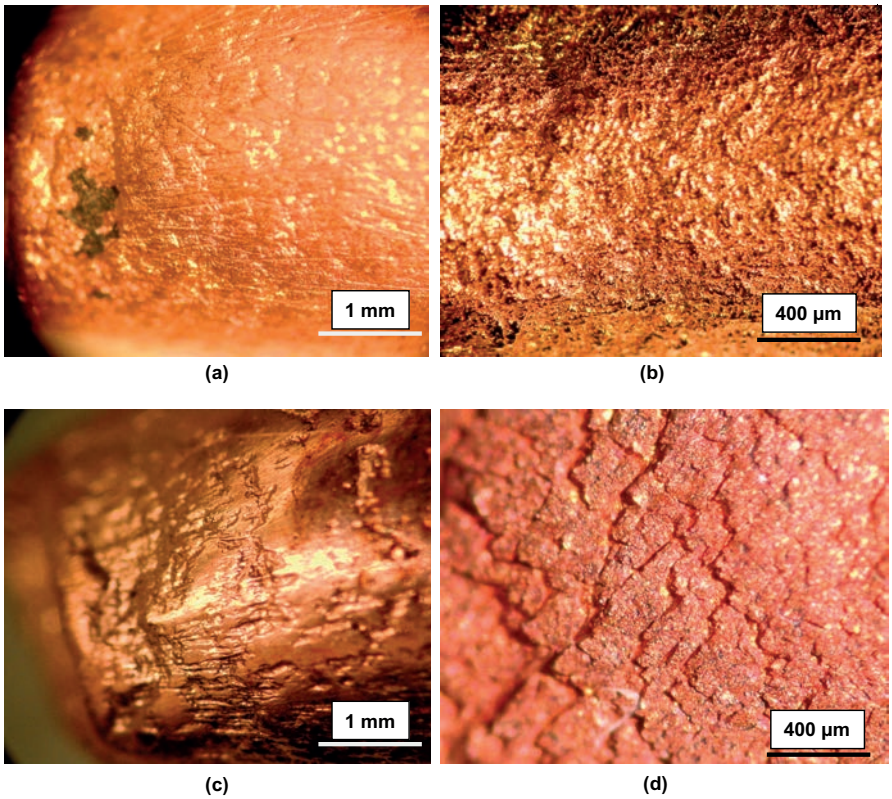

Figure 3-4. *Morphology of the exposed surface of copper SSRT specimens after removing the sulfide film, under the experimental conditions ((a) through (d)) of Test 7, Test 9, Test 16 and Test 17 as shown in Table 3-1. The zig-zag patterns are probably due to enhanced corrosion at sites of film fracture.*

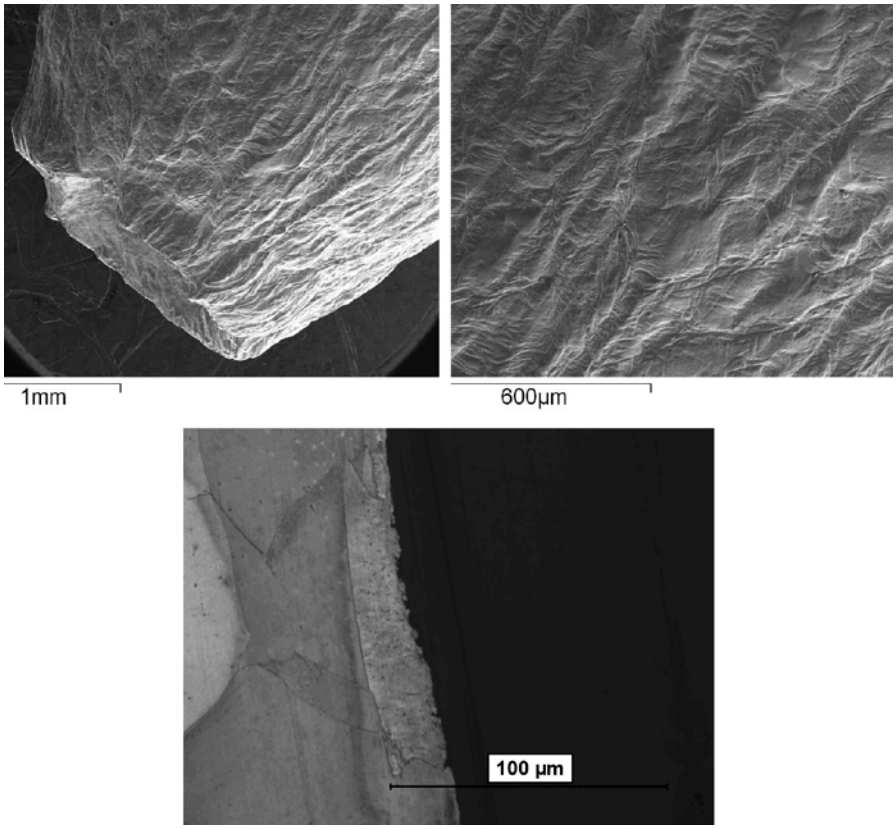

Figure 3-5. *Surface and longitudinal cross section of the tensile specimen tested in synthetic seawater with addition of 10 mM Na_2S at room temperature, obtained in Test 19.*

3.2 Electrochemical behaviour

3.2.1 Open circuit potentials and polarization curves

SKB copper in 100 mM chloride solution had an OCP of ca –0.49 V (MSE) in nominally deaerated conditions for pH near 7 at room temperature. After adding 10 mM Na_2S, the OCP moved instantly to ca –1.38 V_{MSE} (equivalent to –965 mV_{SCE}) and sulfidation visibly occurred within a few seconds. :

$2Cu + HS^- \rightarrow Cu_2S + H^+ + 2e^-$ (anode)

$2H_2O + 2e^- \rightarrow H_2 + 2OH^-$ (cathode)

The pH of the solution made in this manner is ca 12.0.

The OCP of the copper specimen in deaerated synthetic sea water with addition of 10 mM Na_2S was also recorded with time, as shown in Figure 3-6. It can be seen that the corrosion potential just after sulfide addition was about the same in both solutions, but more dynamic change happened with time in synthetic sea water. The pH of this solution was also lower, and $CaCO_3$ was precipitated.

Using a copper specimen from Alfa Aesar, potentiodynamic polarization studies were carried out in the potential window of –1.2 to 0.1 V_{SCE} at a scan rate of 1 mV/s in synthetic seawater with addition of 10 or 20 mM Na_2S at 80°C as shown in Figure 3-7. Black precipitate (corrosion product Cu_2S) could be seen at the bottom of the cell at the end of the scan. In the potential region of –900 to –100 mV the current remains almost constant, indicating diffusion control by inward diffusion of sulfide ions, with the location of the diffusion control being a series combination of solution boundary layer and pores in the film. This was consistent with little elongation difference observed between Tests 25 and 26 in Figure 3-2, which were done at different anodic polarization potentials. In the absence of cracking, reduction in elongation is due to section loss by corrosion. However the effect of bulk sulfide concentration on sulfidation rate or apparent mechanical properties is not necessarily a simple proportionality, as different sulfide concentrations give different film morphologies and thus different influence of the film porosity.

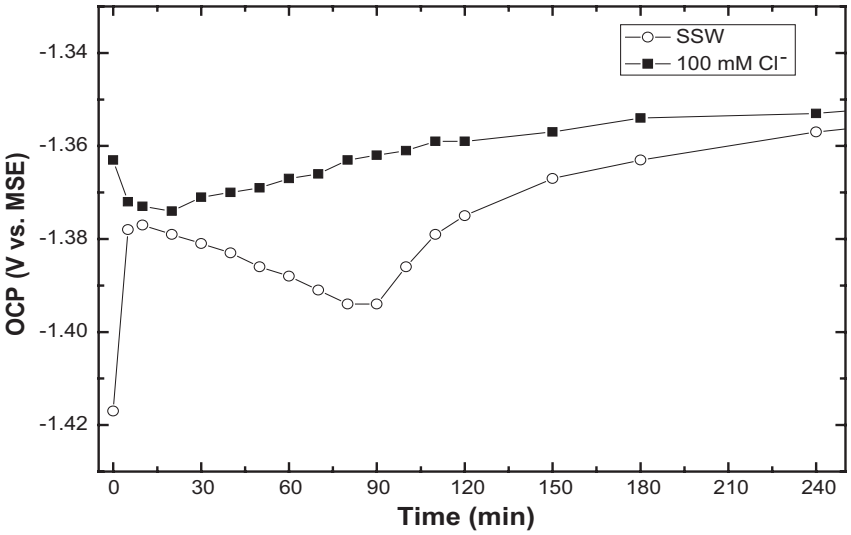

Figure 3-6. *Open circuit potential vs. time curves of SKB copper specimens in 100 mM NaCl solution and synthetic sea water (SSW, ca 500 mM chloride) with addition of 10 mM Na_2S at room temperature. (MSE = 0.40 V vs SCE)*

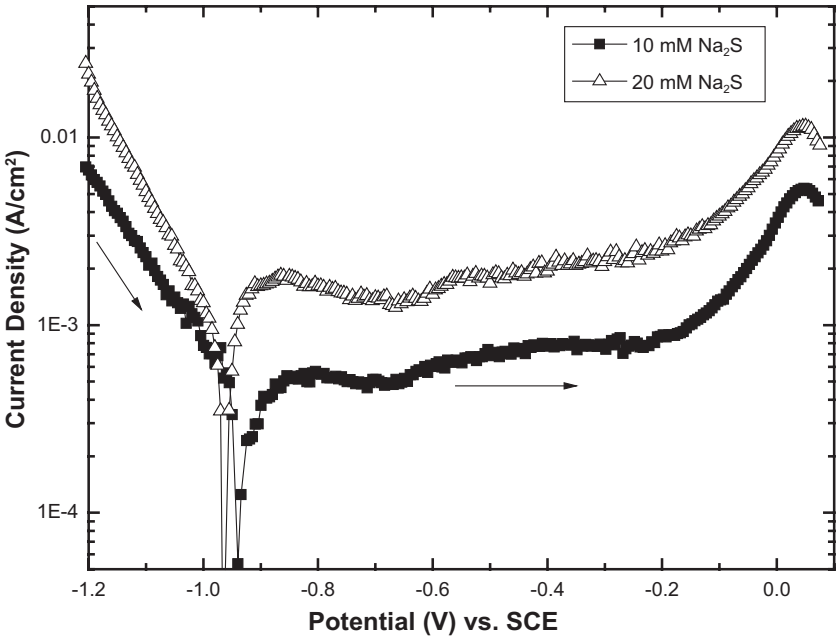

Figure 3-7. *Potentiodynamic polarization curves of SKB copper specimens in synthetic sea water with addition of 10 mM and 20 mM Na_2S at 80°C.*

3.2.2 Impedance measurement

Corresponding to Figure 3-6, electrochemical impedance data at different immersion times at room temperature in 100 mM NaCl solution and synthetic sea water, both with addition of 10 mM Na_2S, are shown in Figure 3-8. It can be seen that, in 100 mM NaCl solution, the polarization resistance increased quickly at the initial stages and became relatively stable after 30 minutes; while in synthetic sea water, it increased quickly and continuously during 60 minutes, and then decreased up to 120 minutes. Based on these data, it is reasonable to think that the corrosion film in the former solution could be relatively more compact, whereas in the latter it is coarser and looser, more easily spalled off. This was also consistent with the observation that, in 100 mM NaCl solution (with addition of Na_2S), the corrosion film was adherent and could not be easily removed for examination of the underlying metal surface. Nevertheless, the data do not give any contradictory information to the notion that corrosion is diffusion-controlled by inward diffusion of sulfide – a lower corrosion rate can always be rationalized by assuming that the dominant diffusion path is through pores in the sulfide film. But it would be unusual to observe a grain orientation effect on corrosion rate, but then conclude that all the corrosion is really diffusion controlled, but that the different corrosion rates on different grains are due to diffusion control through films of different porosity (not that this is impossible in principle). Normally such grain orientation effects are ascribed to different reaction kinetics.

Impedance spectra from a longer immersion test in 100 mM NaCl solution with the addition of 5 mM Na_2S are shown in Figure 3-9. Such data tend to confirm that the corrosion film was relatively compact and that the corrosion process was under diffusion control, predominantly within the pores of this film, after some duration of corrosion.

The effect of stirring on the impedance spectra in synthetic sea water with the addition of 10 mM Na_2S is shown in Figure 3-10. The stirring control procedure was shown in Figure 2-2. Generally speaking, such data show that stirring relieves the diffusion control of the corrosion reaction, but the interpretation can be complex, because stirring also reduces the film growth (deposition?) rate and even shears off the more fragile outer part of the film, so that the effect of an on-off cycle of stirring may not be reversible.

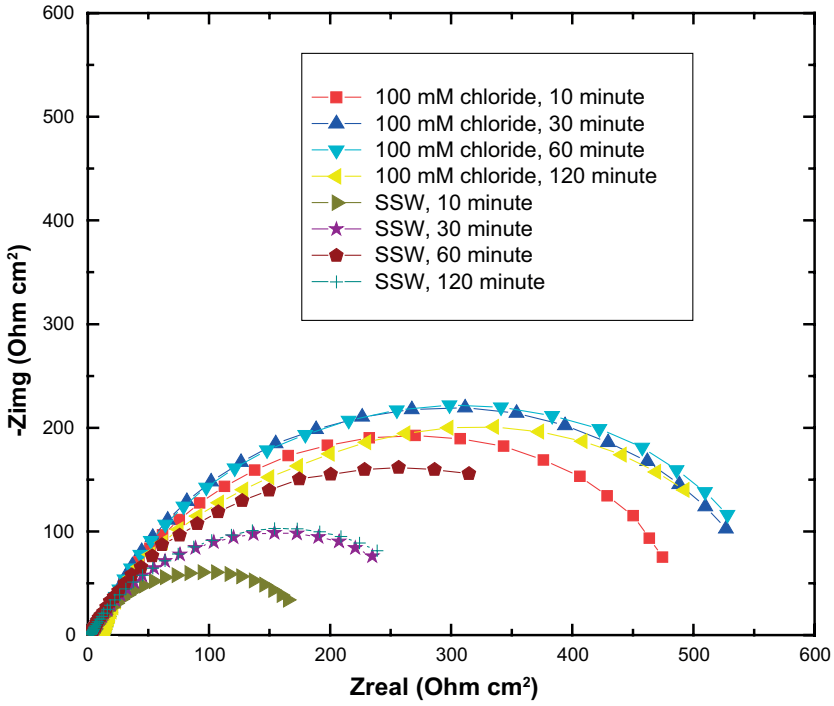

Figure 3-8. *Nyquist electrochemical impedance spectra for SKB copper at different immersion times in 100 mM NaCl solution and in synthetic sea water (SSW, ca 500 mM chloride) with addition of 10 mM Na_2S at room temperature. Frequency range: 100 kHz – 0.1 Hz. The pH was unadjusted in both solutions.*

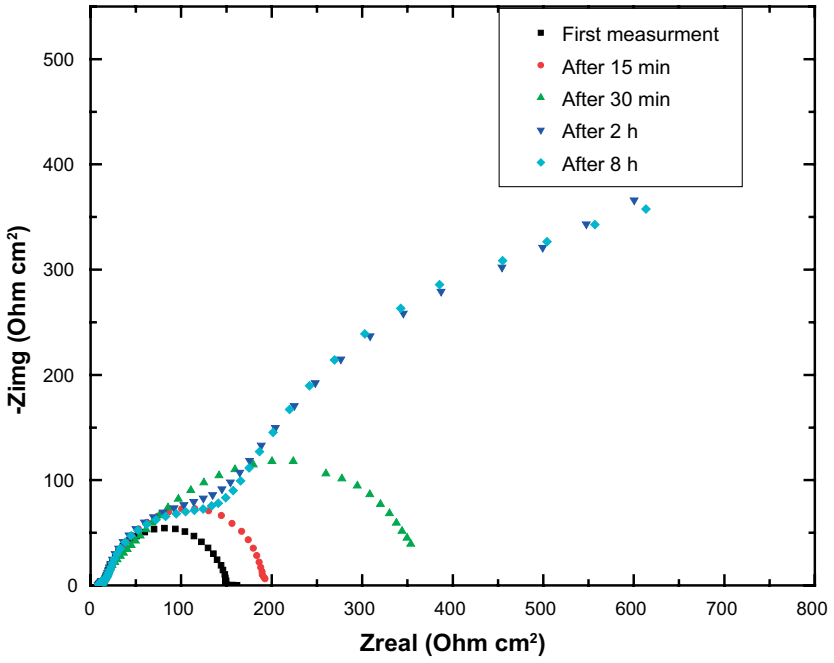

Figure 3-9. *Impedance spectra of SKB copper specimen after longer immersion in 100 mM NaCl solution with addition of 5 mM Na_2S at room temperature. Frequency range: 100 kHz–0.1 Hz.*

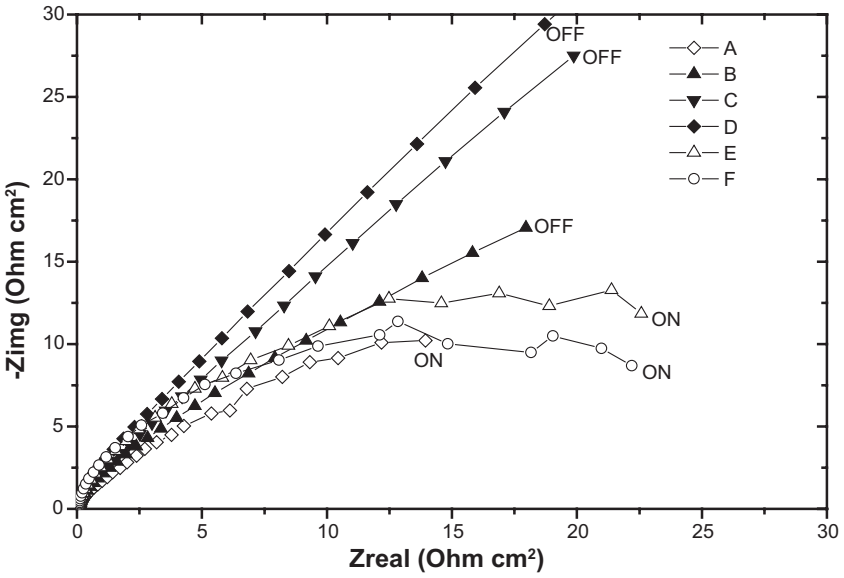

Figure 3-10. *Effect of stirring on the impedance behavior of the SKB copper specimen in synthetic sea-water with addition of 10 mM Na_2S at room temperature, according to the programme shown in Figure 2-2. Frequency range: 100 kHz–0.1 Hz.*

3.2.3 Intermediate corrosion products

The sulfidation reaction of copper occurs without obvious dissolution of the copper ions. Smith proposed that the sulfidation reaction of the copper in aqueous solution involves the formation of soluble complexes (Smith 2007), but these were not detected by in situ Raman spectroscopy. As discussed earlier, published stability constants for such complexes, although large, do not support their formation at the observed corrosion potentials; on the other hand, the manner of porous film formation in this system does seem very typical of a dissolution-reprecipitation process. Using the setup shown in Figure 2-3, cyclic voltammetry was done on the small gold electrode in synthetic sea water with addition of 10 mM Na_2S at room temperature. The potential scan rate was 50 mV/s and the potential window was –1.2 to 0.1 V vs. SCE. A separate scan was made in sulfide-free solution for reference. No evidence for soluble Cu was found, although the work was preliminary and further work using smaller electrodes would be beneficial to elaborate this point.

3.3 Constant strain tensile testing and simple immersion tests

3.3.1 Tests on tensile specimens with constant strain

In view of the possibility that potentials in published work showing SCC might be more oxidizing than expected for a properly deoxygenated system, some immersion testing and constant-strain exposure was carried out without deliberate deaeration, i.e. with some elemental sulfur and/or thiosulfate present (these amounts would be small, as the system was sealed with its initial amount of dissolved oxygen, i.e. ca 8 ppm).

The surface morphologies of the gauge part of the tensile specimen and specimen A (unstressed) in 10 mM H_2S water at room temperature without deaeration are shown in Figure 3-11 and Figure 3-12. The corrosion product could be removed very easily in an ultrasonic bath. No SCC was found. Despite the presence of oxidized species, the behaviour was very similar to that in deoxygenated solution – a bilayer film, well shown in Figure 3-11d.

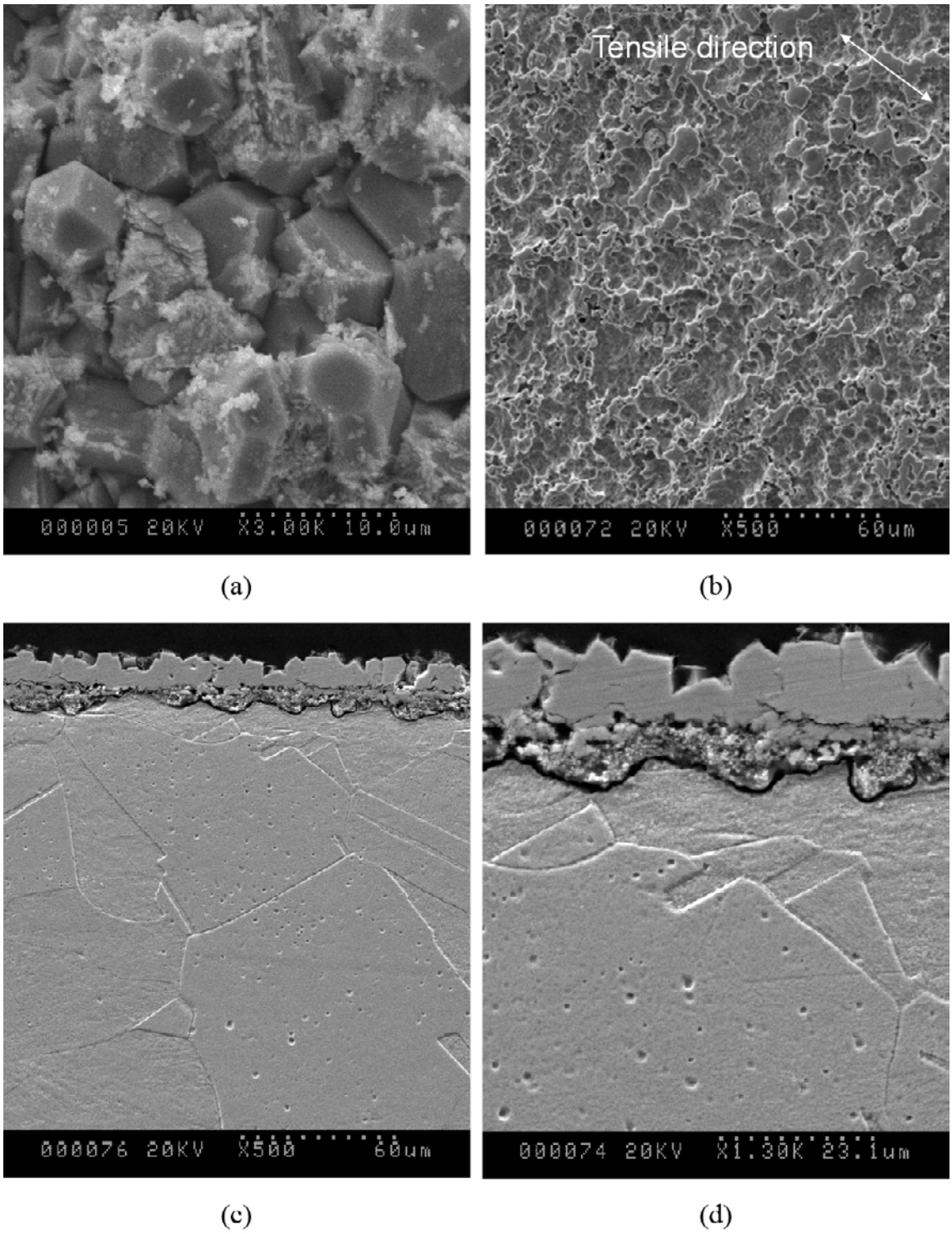

Figure 3-11. *Surface morphology of the gauge part of the tensile specimen used for constant-strain SCC testing (strain 2.4%) and its cross section: (a) – with corrosion film; (b) – corrosion film removed in ultrasonic bath; (c) and (d) – longitudinal cross section with different magnification. Test solution: 0.01 M H_2S in water without deaeration.*

Regarding the importance of diffusion control by inward sulfide diffusion, the pit-like attack seen in Figure 3-12b might constitute a counter-argument to such rate control (the dissolution rate within a cavity would normally slow down with time if it is under diffusion control), but it is very shallow. If the metal surface within such 'pits' carries a thinner or more openly porous film, there might be a modestly higher corrosion rate despite the nominal geometry favouring corrosion on the flat surface.

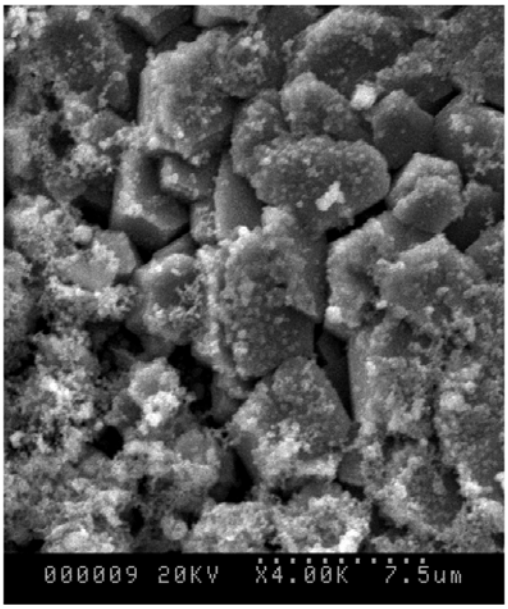

(a)

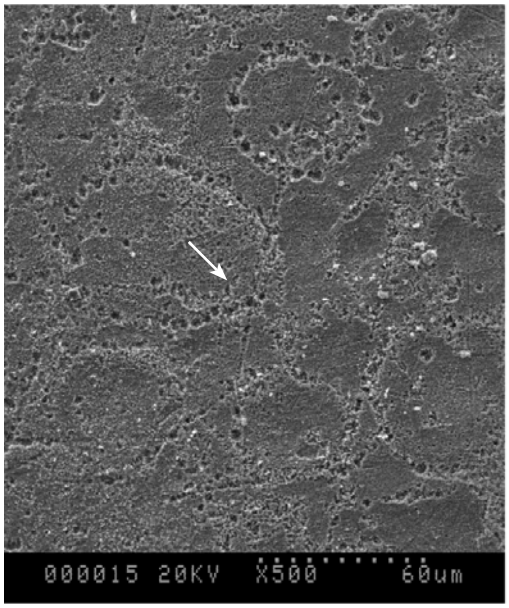

(b)

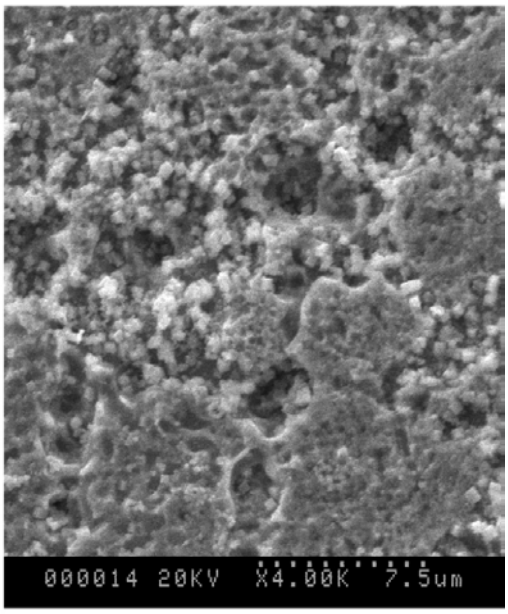

(c)

Figure 3-12. *Surface morphology of copper specimen A before (a) and after (b) the corrosion product film was removed in an ultrasonic bath. Image (c) shows a detail from (b) as indicated by the arrow in (b). Test solution: 0.01 M H_2S in water without deaeration.*

A comparison with Figure 3-13 and Figure 3-14 shows that deoxygenation had little or no effect on the corrosion behaviour as deduced from film morphology. The films were a little less fragile but otherwise similar. Wherever there was some indication of intergranularity (e.g. Figure 3-14b), it turned out to be superficial on closer examination. In any event, there was no evidence of SCC and no evidence of deep, penetrating intergranular corrosion.

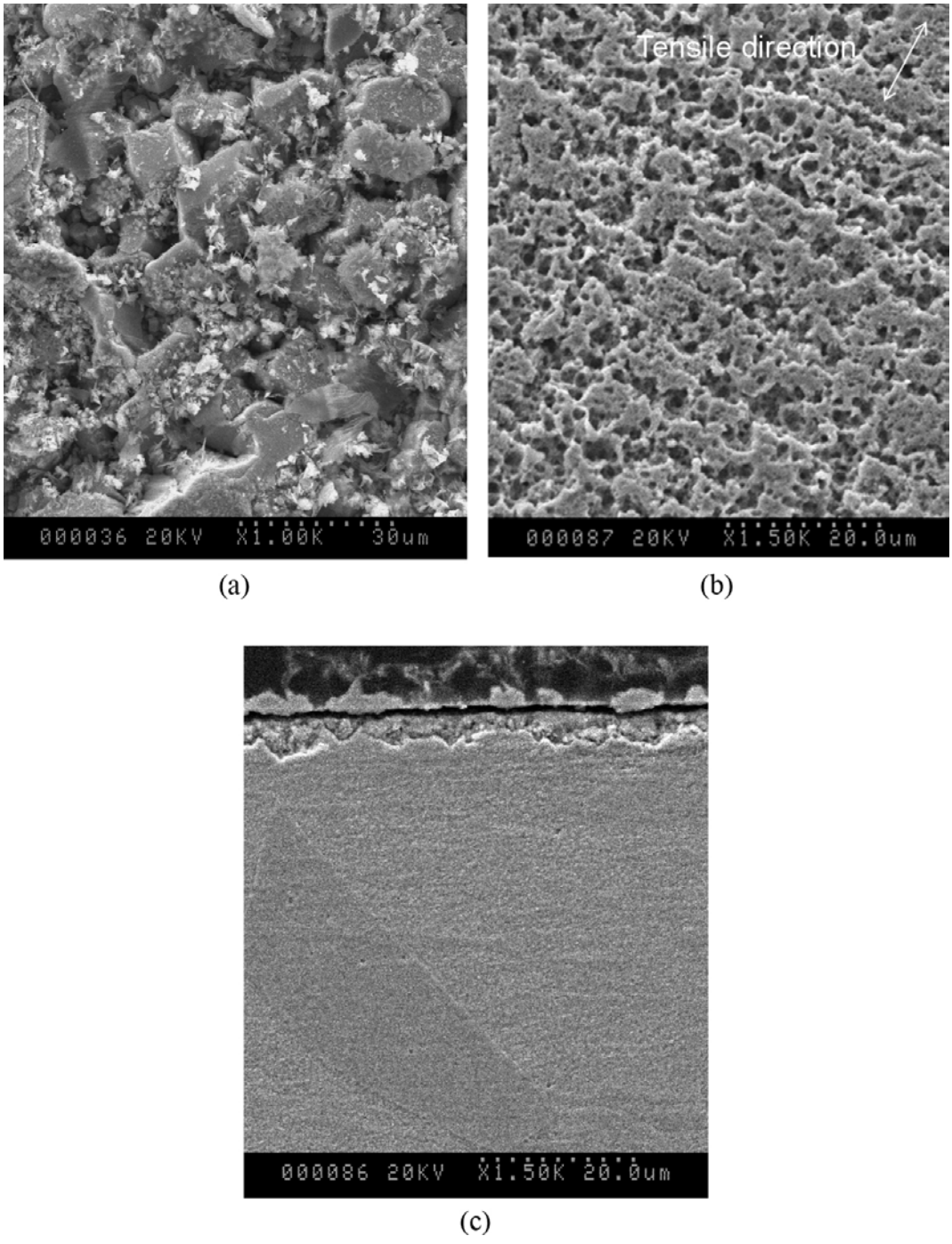

Figure 3-13. *Surface morphology of the gauge part of the tensile specimen used for constant-strain SCC testing (strain 9.2%) and its cross section: (a) – with corrosion film; (b) – corrosion film removed in ultrasonic bath; (c) – cross section. Test solution: 0.01 M H_2S in water with deaeration.*

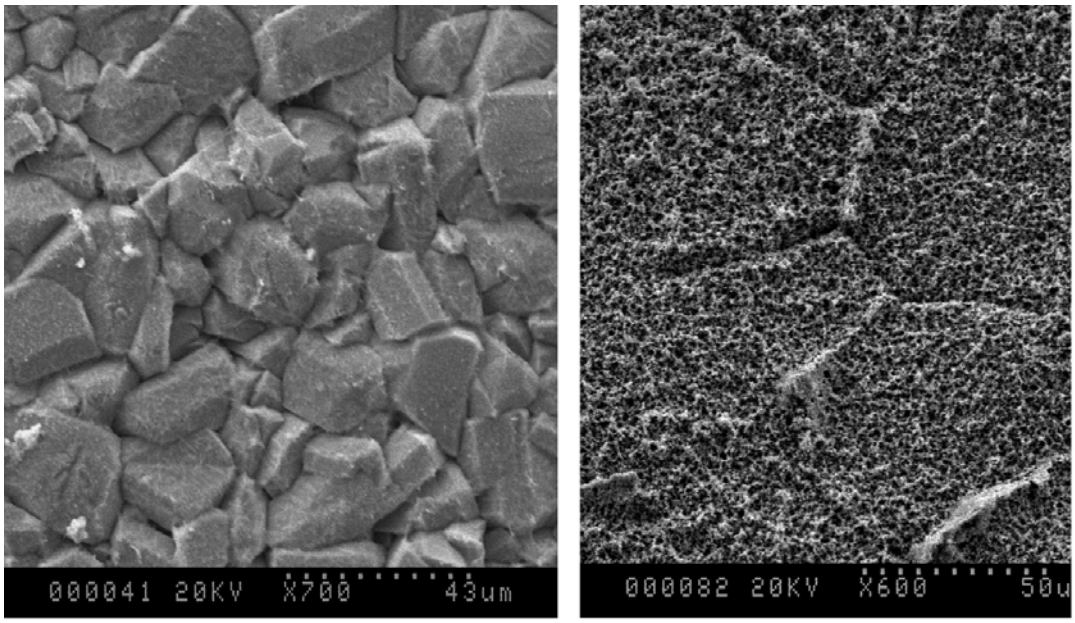

Figure 3-14. *Surface morphology of copper specimen B before and after its corrosion film was removed in an ultrasonic bath; (a) – before; (b) – after. Test solution: 0.01 M H_2S in water with deaeration.*

3.3.2 Tests on U-bend specimens

This testing was designed to give the maximum possible excellence of deaeration, together with relatively severe stress and strain conditions. Solutions of 0.5 M NaCl + 10 mM Na_2S and 0.5 M NaCl + 100 mM Na_2S were used. The bend surface of a U-bend specimen before immersion is shown in Figure 3-15. Slip bands and their interactions with grain boundaries can be observed, as can the scratch lines produced by 1 µm diamond paste. The bend surfaces of the U-bend specimens after immersion in 0.5 M NaCl + 10 mM Na_2S and 0.5 M NaCl + 100 mM Na_2S are then shown in Figure 3-16 and Figure 3-17 respectively.

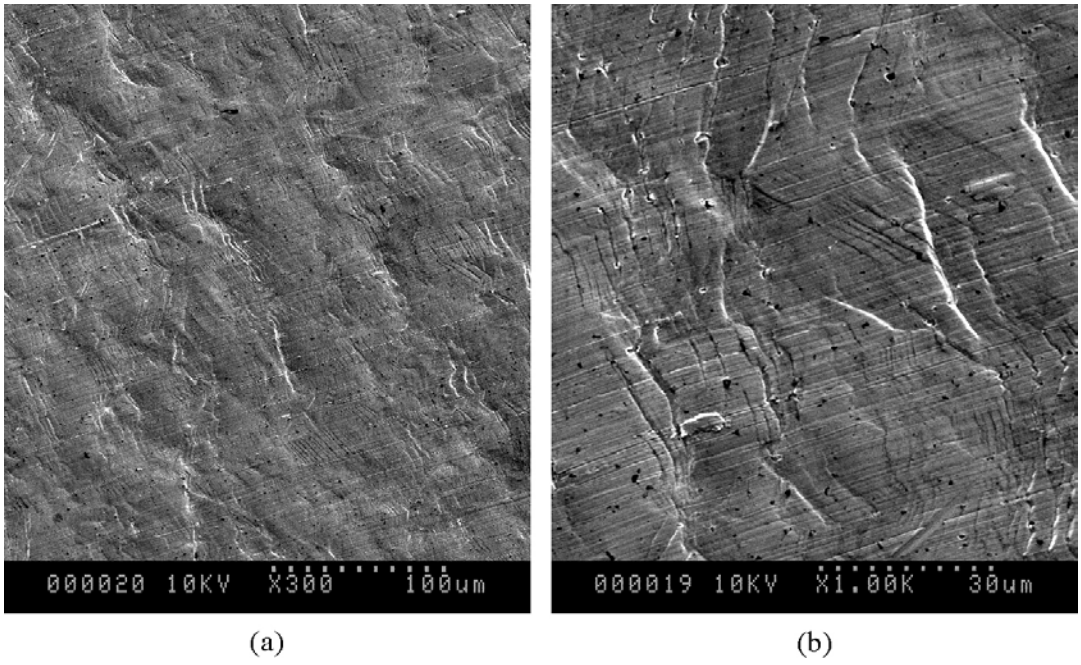

Figure 3-15. *The outside bend surface of one U-bend specimen before testing. The surface was ground and polished down to 1 um diamond paste and severely bent (40–50% strain at the bend apex surface): (a) and (b) at different magnification.*

This testing was done late on in the project, and it was not possible to ascertain whether the thin films formed in these conditions were, in whole or in part, the result of improved deaeration. However this feature is certainly striking, and it is clear that if inward sulfide diffusion does indeed control the corrosion rate, the pores in the thin sulfide film must be the main diffusion barrier, not the bulk solution. The films could not completely be removed after 30 minutes in an of ultrasonic bath (only part of the outside layer was removed). No SCC was found. (In Figure 3-16c, the surface is very smooth, because the specimen was first bent and then polished).

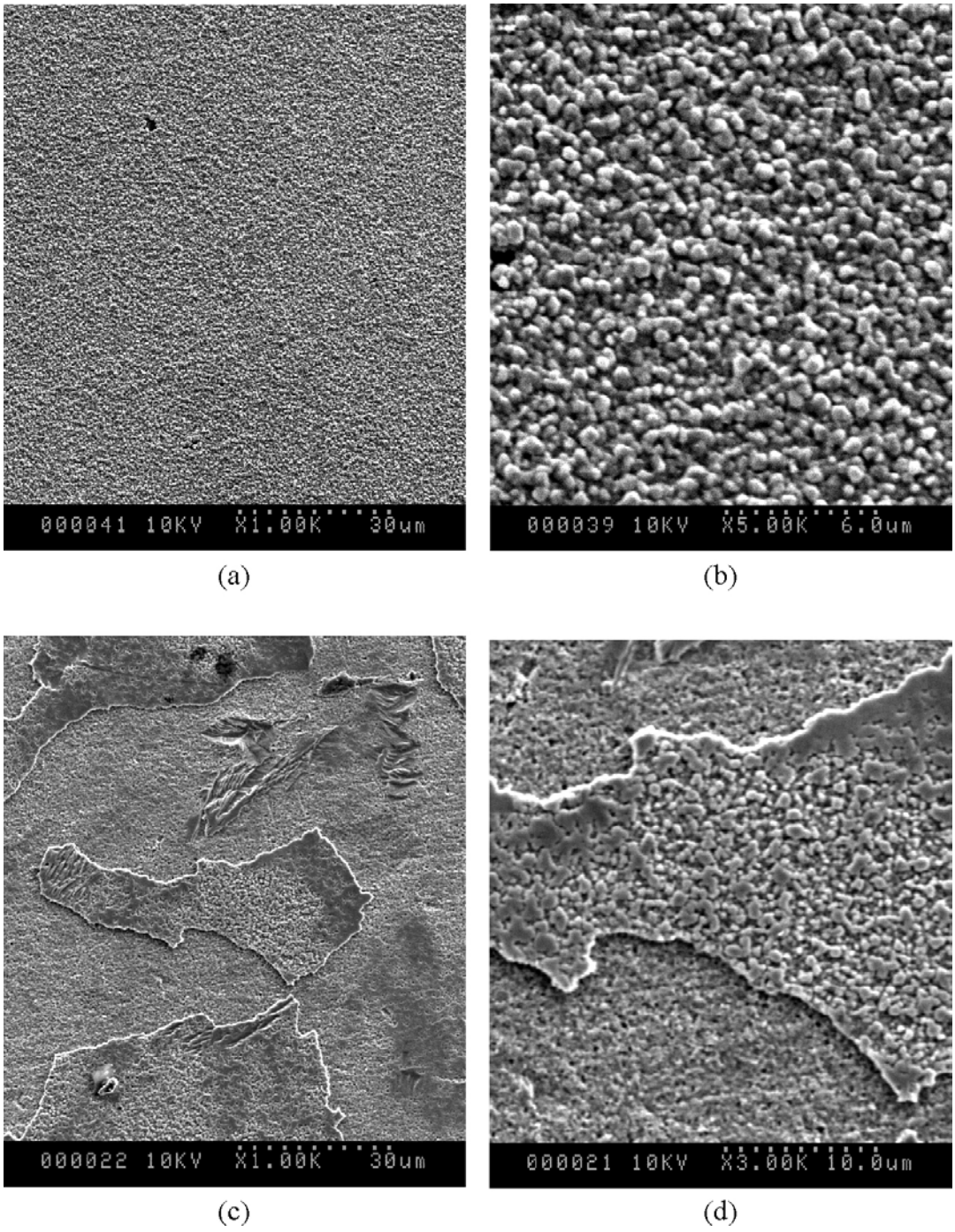

Figure 3-16. *The outside bend surface morphology of a U-bend specimen after immersion testing in solution of 0.5 NaCl + 0.01 M Na_2S : (a) and (b) – with corrosion film (different magnifications); (c) and (d) – corrosion film partly removed in ultrasonic bath (different magnifications).*

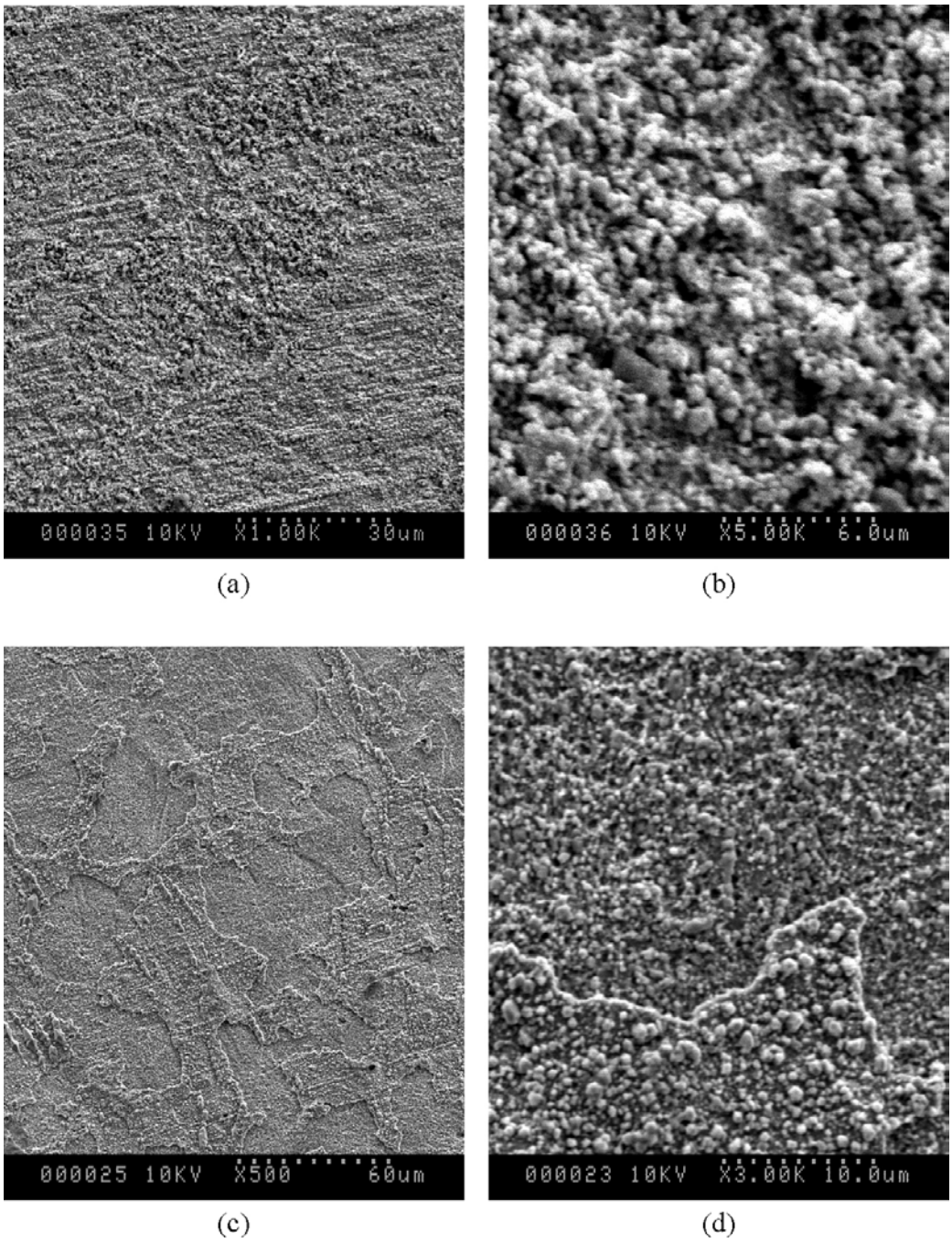

Figure 3-17. *The outside bend surface morphology of a U-bend specimen after immersion testing in solution of 0.5 NaCl + 0.1 M Na_2S : (a) and (b) – with corrosion film (different magnifications); (c) and (d) – corrosion film partly removed in ultrasonic bath (different magnifications).*

3.3.3 Tests on specimens with punch indents, near and far from the indent; effect of grain orientation on corrosion

No cracking was found in the electropolished, then punched, specimens in synthetic sea water with addition of 2 mM, 10 mM or 50 mM Na_2S. The surface morphology near the punch dent of the specimen in synthetic sea water with addition of 2 mM Na_2S is shown in Figure 3-18. The difference in film thickness on differently oriented grains is clearly seen.

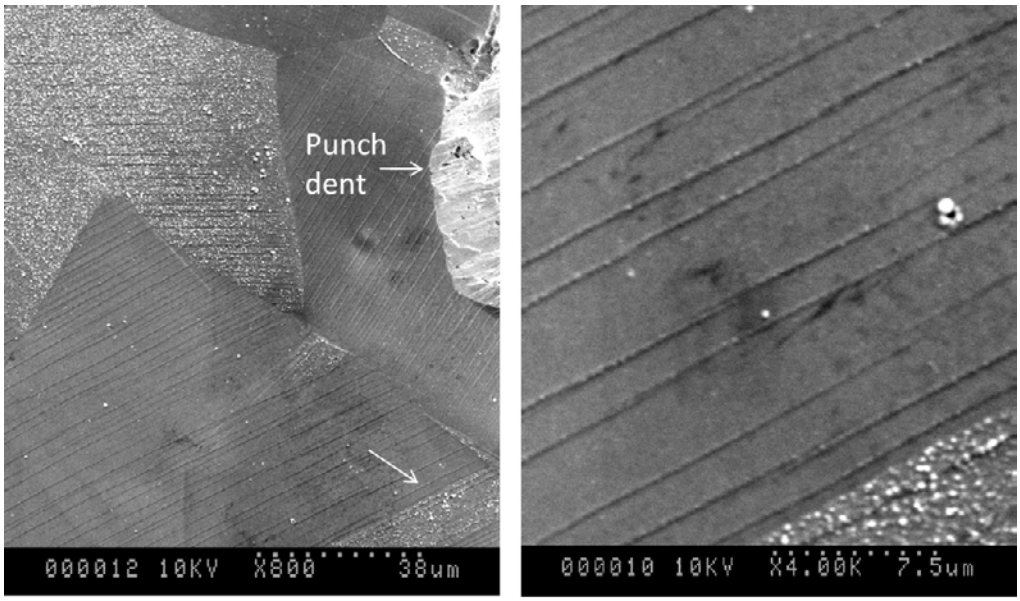

Figure 3-18. *The surface morphology near the punch dent of the specimen after immersion in synthetic sea water with addition of 2 mM Na_2S; (b) – area indicated by arrow in (a).*

By examining an area away from the punch indent, a similar result was obtained without influence of plastic deformation – Figure 3-19. The impression of differences in thickness of the Cu_2S film was confirmed by EDX analysis (Figure 3-19g–j), which also confirmed that no other elements were present apart from S and Cu. Deducing film thickness from such data is not an exact science, but the film analyzed in Figure 3-19j must be less than 50 nm thick, while the thickest films are microns thick.

Such results suggest that sulfide film formation is highly dependent on grain orientation, i.e. that there is some epitaxy effect, which was explored further by EBSD analysis. Again, this would normally be taken as evidence that diffusion in the solution phase is not rate-controlling, but this is not certain – one can imagine a sequence where film nucleation is controlled by crystallography, creating more, or less, dense arrays of film nuclei; then as these develop into a porous film, they retain a memory of their starting configuration and allow more, or less, inward diffusion of sulfide.

The same specimen was also analyzed with AES in a number of areas. The first analyzed area and set of AES data are shown in Figure 3-20 – the darker area corresponds to a thinner film. This specimen had already been carbon coated for SEM before AES analysis, so the carbon signal is very strong before sputtering. The oxygen signal is weak, particularly after sputtering. The main elements existing in the surface film are S and Cu. With sputtering (depth), in area 2, the sulfur signal decreased after a while; while in area 1, the sulfur signal was almost constant. This confirms that the thickness of the Cu_2S corrosion film was different depending on grain orientation. No attention should be paid to the atomic percentages of S and Cu quoted in Figure 3-20b–c – standards were not available for proper calibration.

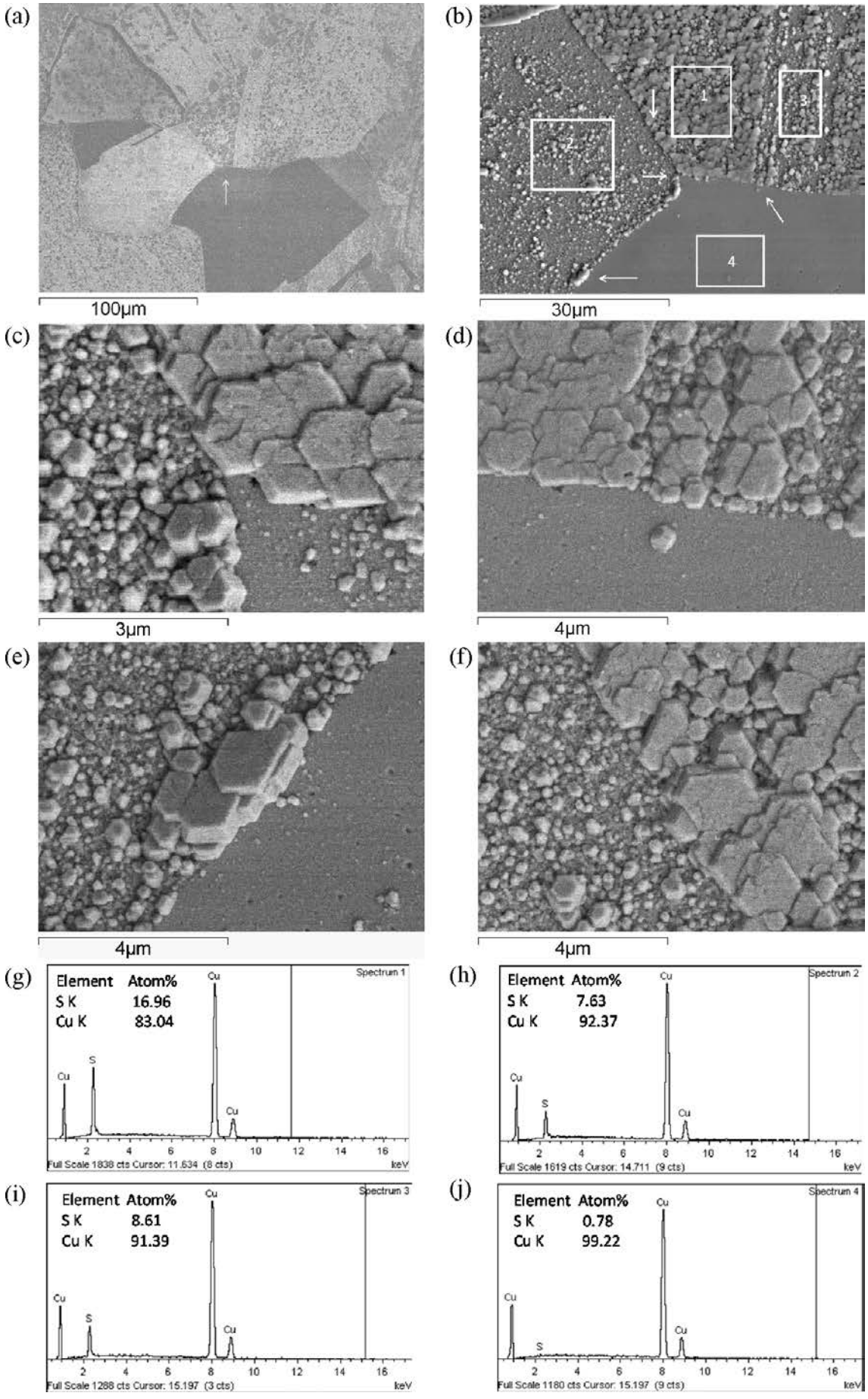

Figure 3-19. *The surface morphology of an area well away from the punch dent after immersion in synthetic sea water with addition of 2 mM Na_2S; (b) – area indicated by arrow in (a); (c), (d), (e), (f) – areas indicated by arrows in (b); (g), (h), (i) and (j) – EDX data obtained from the respective areas in (b).*

(a)

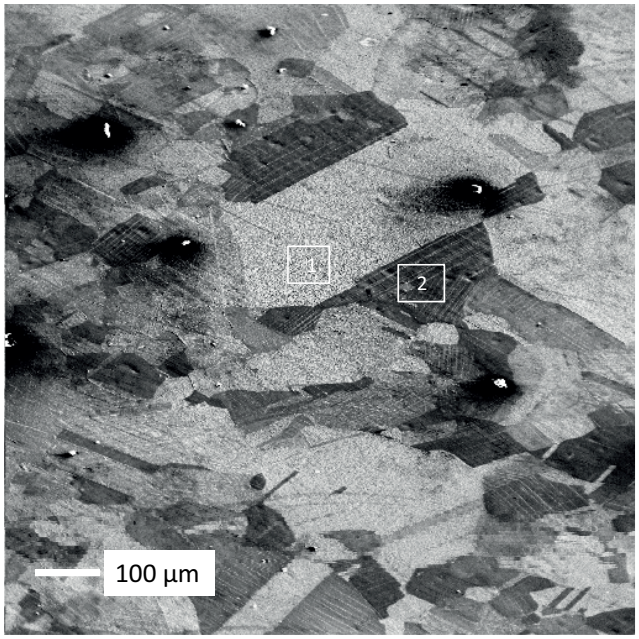

(b)

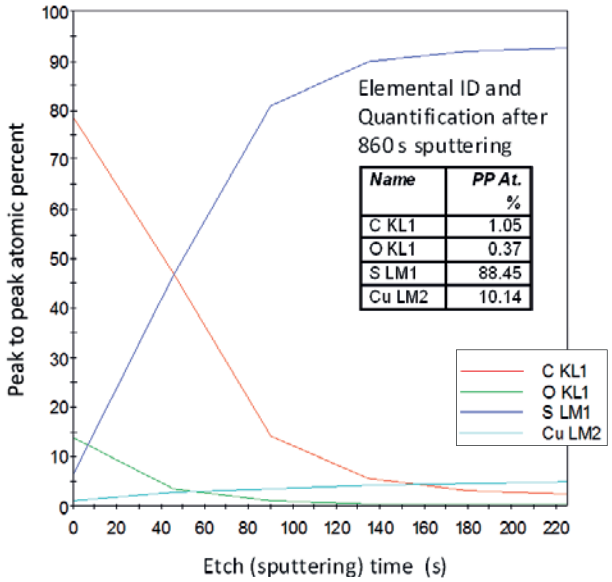

(c)

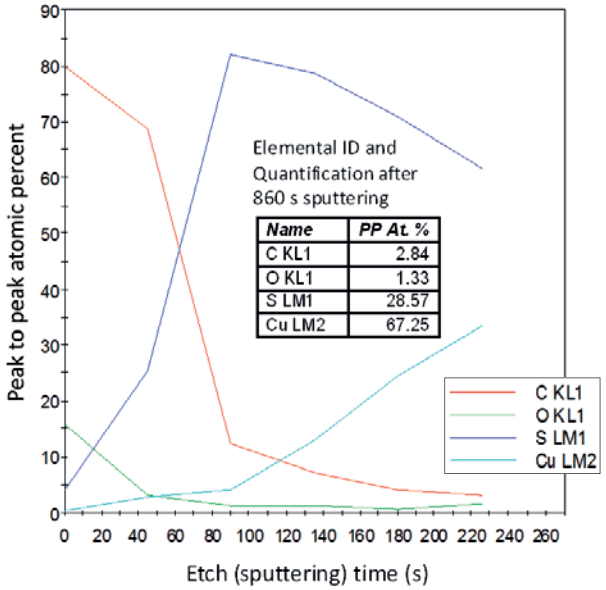

Figure 3-20. *AES analysis on the surface of the specimen immersed in synthetic sea water with addition of 2 mM Na_2S; (a) – analyzed areas; (b) and (c) – sputter depth profiles in areas 1 (thicker film) and 2 (thinner film).*

A further campaign on the same specimen produced the data in Figure 3-21 to Figure 3-23. Now the carbon has been removed from the analysis, and the differences in film thickness are clearly shown. One aspect that is not clear is the correlation between the AES and the EDX analyses. The AES showed only a difference of about a factor of 3 between the thinnest and thickest areas, whereas EDX showed much larger differences. This may be related to the different area analyzed and/or to differential sputtering of the compact and loose, particulate, films. It is also possible that when analyzing a porous surface, SEM-EDX has a kind of projection effect where the incident electrons strike the bottom of many or all of the pores.

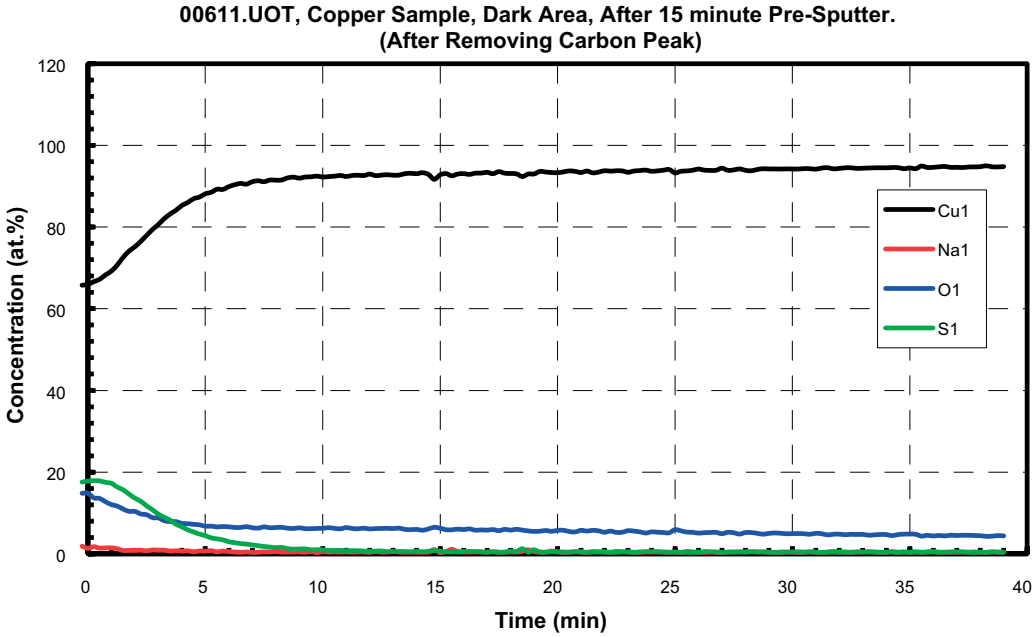

Figure 3-21. *AES sputter depth profile for a darker area (thinner film) with carbon removed. Quantification is obviously affected by the presence of carbon, but the extent of the film is well shown.*

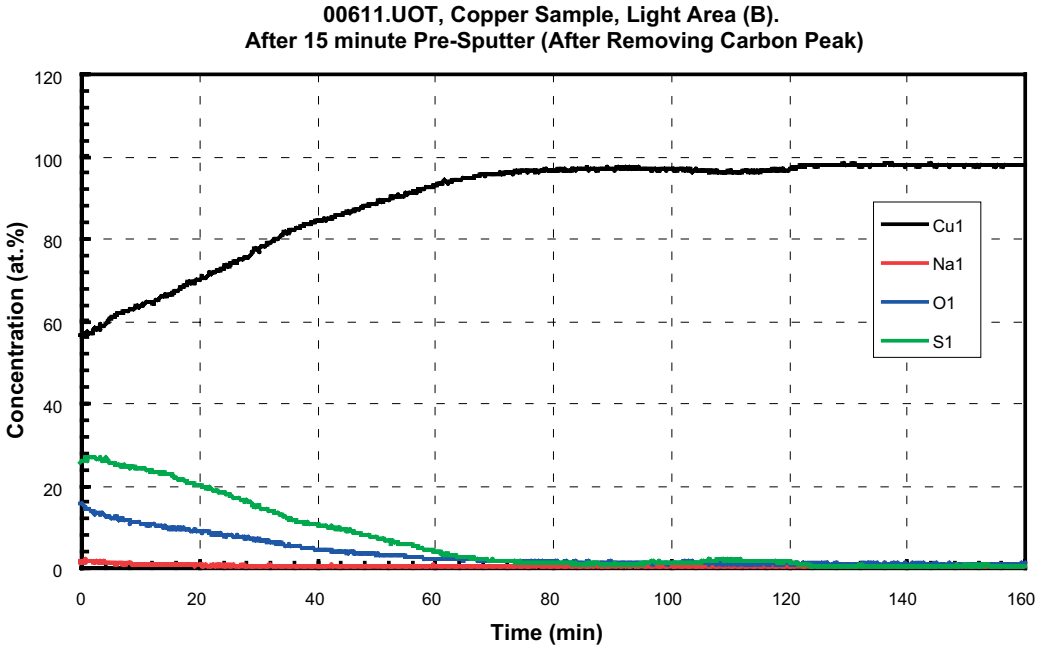

Figure 3-22. *AES sputter depth profile for a lighter area (thicker film) with carbon removed. Quantification is obviously affected by the presence of carbon, but the extent of the film is well shown.*

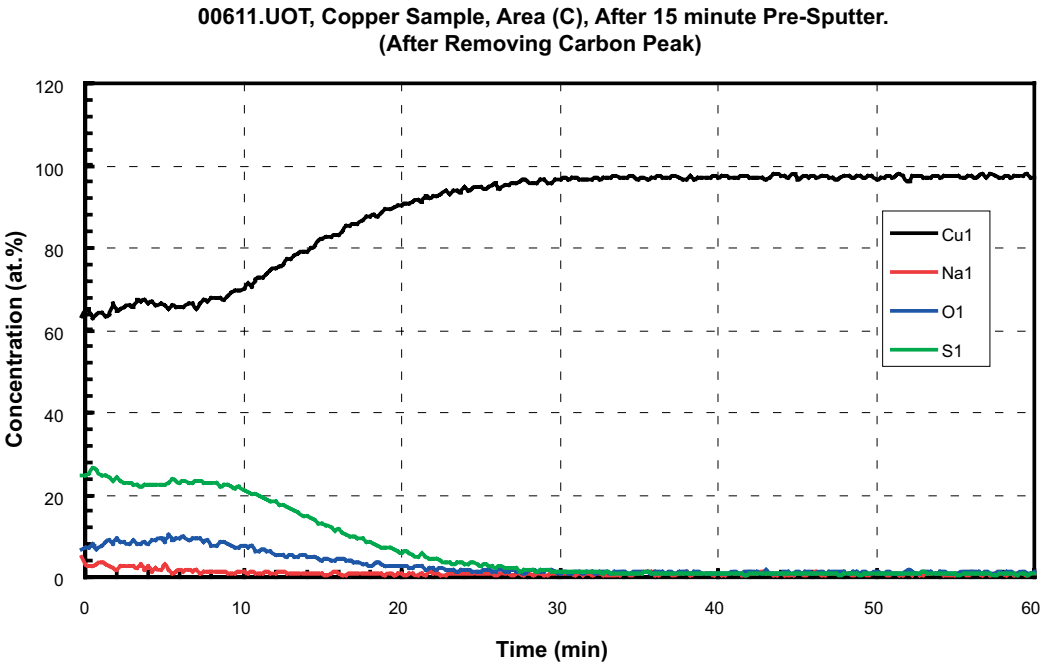

Figure 3-23. *AES sputter depth profile for another lighter area (thicker film) with carbon removed. Quantification is obviously affected by the presence of carbon, but the extent of the film is well shown.*

The same grain orientation effect occurred on the specimens immersed in 10 mM and 50 mM Na_2S in synthetic sea water, as exemplified by Figure 3-24, which is from the 50 mM Na_2S experiment. EDX analysis showed similar results to those found for 2 mM, but the areas of extremely thin film were less prevalent, and the film appearance generally was different, with more evidence of loosely adherent material.

The apparent intergranularity seen in some areas of several of these SEM micrographs is mostly due to the abutting of films of different thickness, formed on adjacent grains. Nothing was seen that could truly be called intergranular corrosion.

The grain orientation effect was not seen, or was weak, in all mechanically prepared specimens.

3.3.4 EBSD examination and correlation of grain orientation with corrosion film development

This part of the study was initially affected by carbon deposited during the EBSD data acquisition, which affected the subsequent corrosion behaviour, as shown by the striping effect in Figure 3-25. The stripes correspond to the positions where the electron beam spent time during the EBSD analysis (they are not really stripes but lines of spots). In order to remove the carbon contamination, it was necessary to do a light electropolish, removing no more than 1–2 microns, after the EBSD (light mechanical polishing was also tried, but was less effective).

In brief, thin sulfide films were seen on grain faces with orientations close to (100) as defined by the colour code shown in Figure 3-26, but also on higher-index faces, and no conclusive overall correlation was found. Figure 3-27 shows one example, while Figure 3-28 illustrates the level of detail that can be achieved. Figure 3-29 shows an example of a particular film morphology that is strongly related to the substrate orientation.

More information is included in Appendix B.

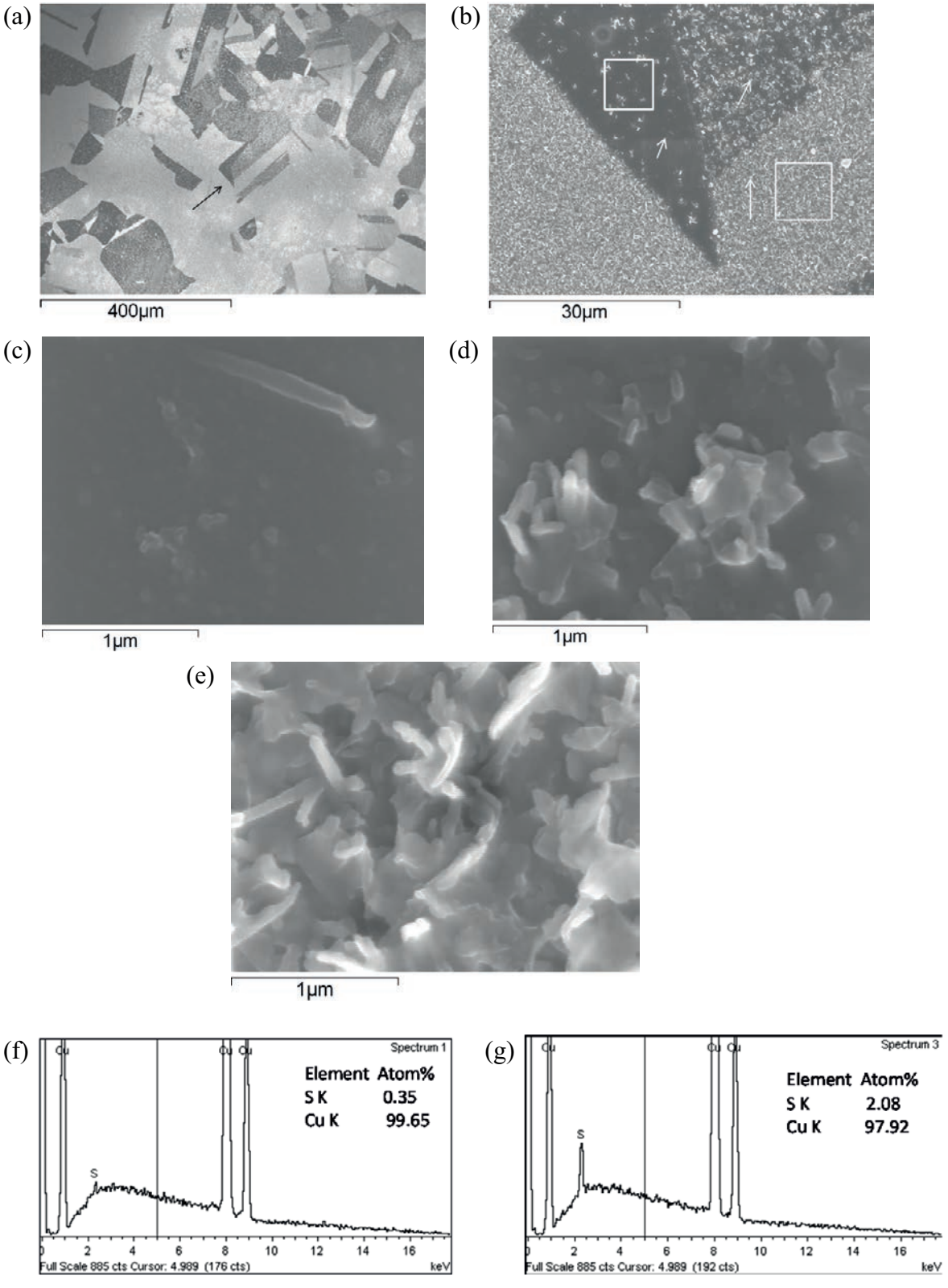

Figure 3-24. *The specimen surface morphology after immersion in synthetic sea water with addition of 50 mM Na_2S; (b) – area indicated by arrow in (a); (c), (d) and (e) – areas indicated by arrows in (b); (f) – EDX data obtained in square marked area in (b) showing thinner film; (g) – EDX data obtained in square marked area in (b) showing thicker film.*

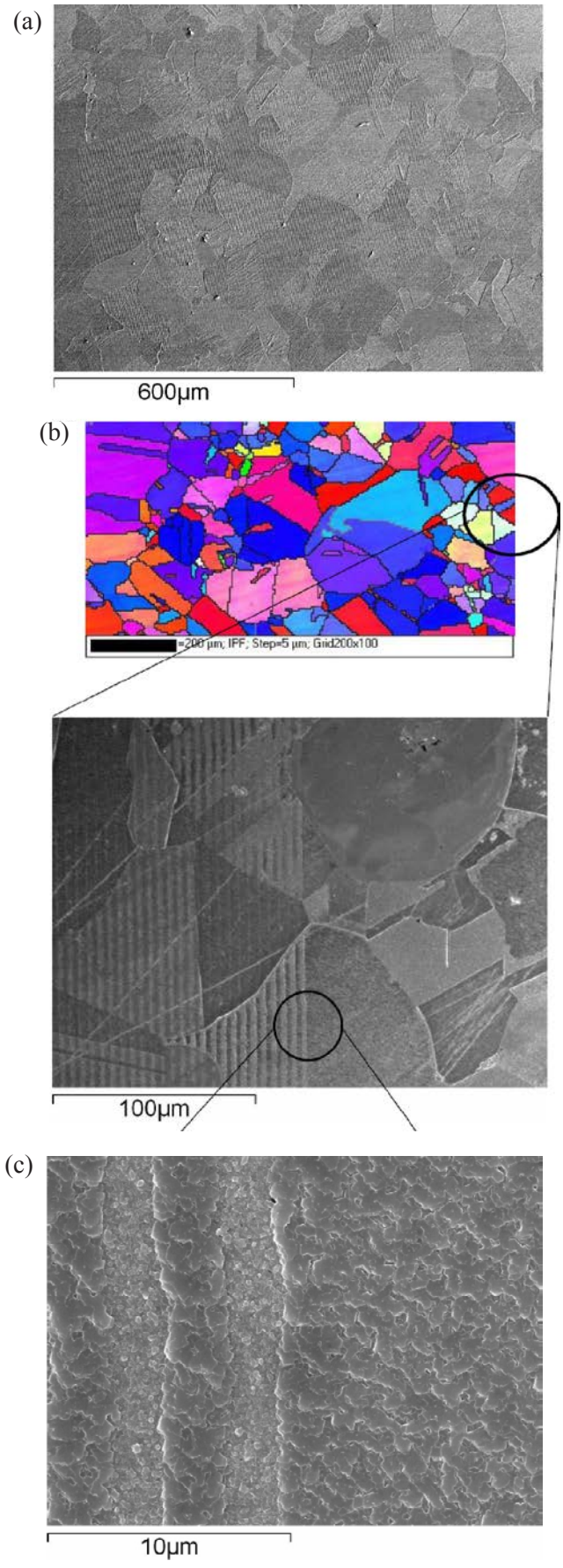

Figure 3-25. *(a) Striped effect obtained after immersion in sulfide solution without cleaning off the carbon deposited during EBSD data acquisition in the trapezoidal area; (b), (c) detail of the edge of the area, corresponding to a fragment of the corresponding orientation map, suggesting that the carbon increases the sulfidation rate.*

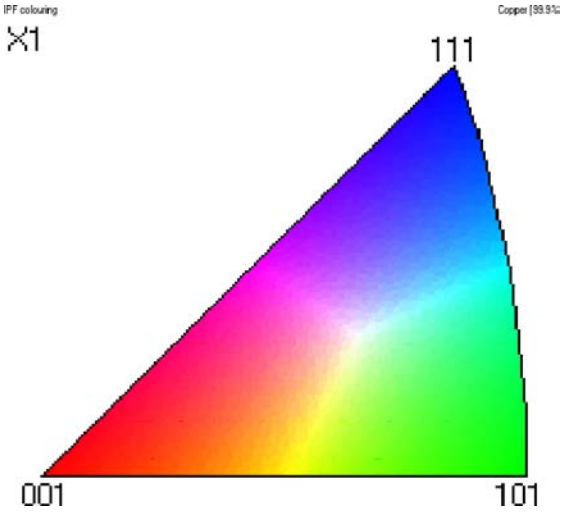

Figure 3-26. *Colour code for the orientation maps (this should not be considered precise).*

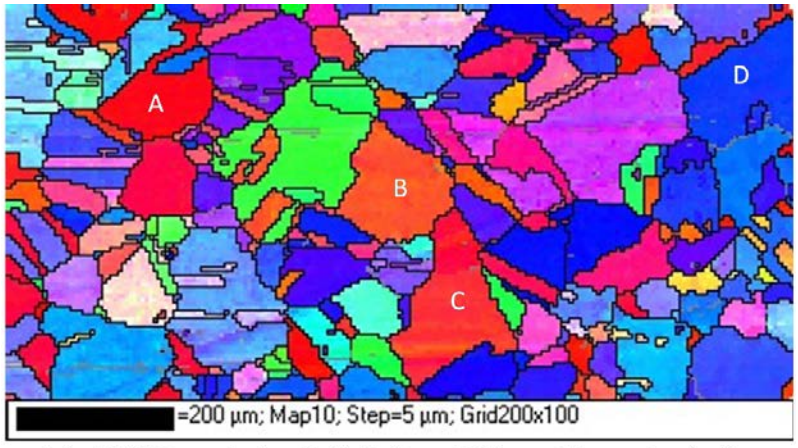

(a) – EBSD image before light electropolishing and immersion testing

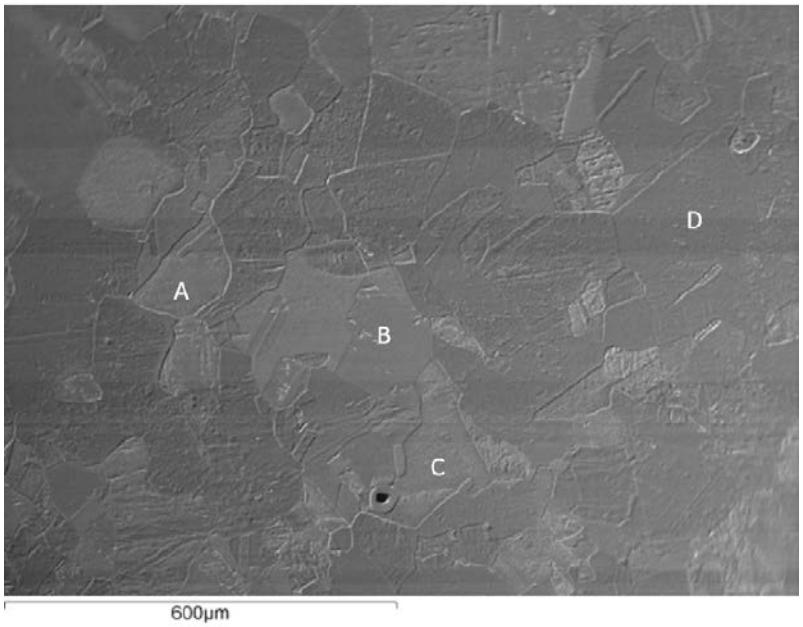

(b) – surface morphology after immersion testing

Figure 3-27. *Example of successful correlation of grain surface orientation with corrosion morphology, for electropolished SKB copper immersed in artificial seawater with 2 mM Na_2S added for 48 hours.*

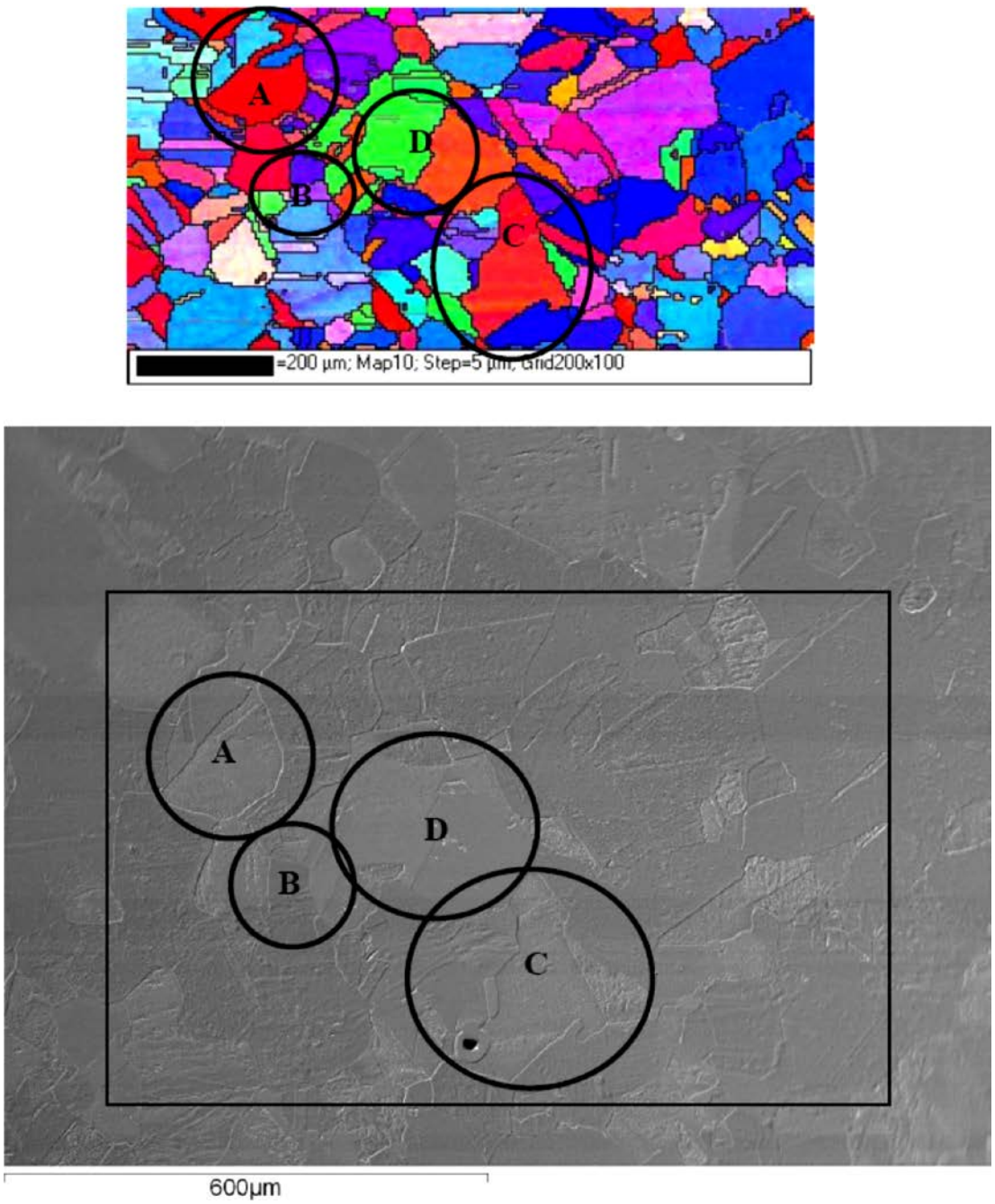

Figure 3-28. *As Figure 3-27, but with detailed characterization of individual areas. A complete set of such analyses is available – see Appendix B.*

Region A

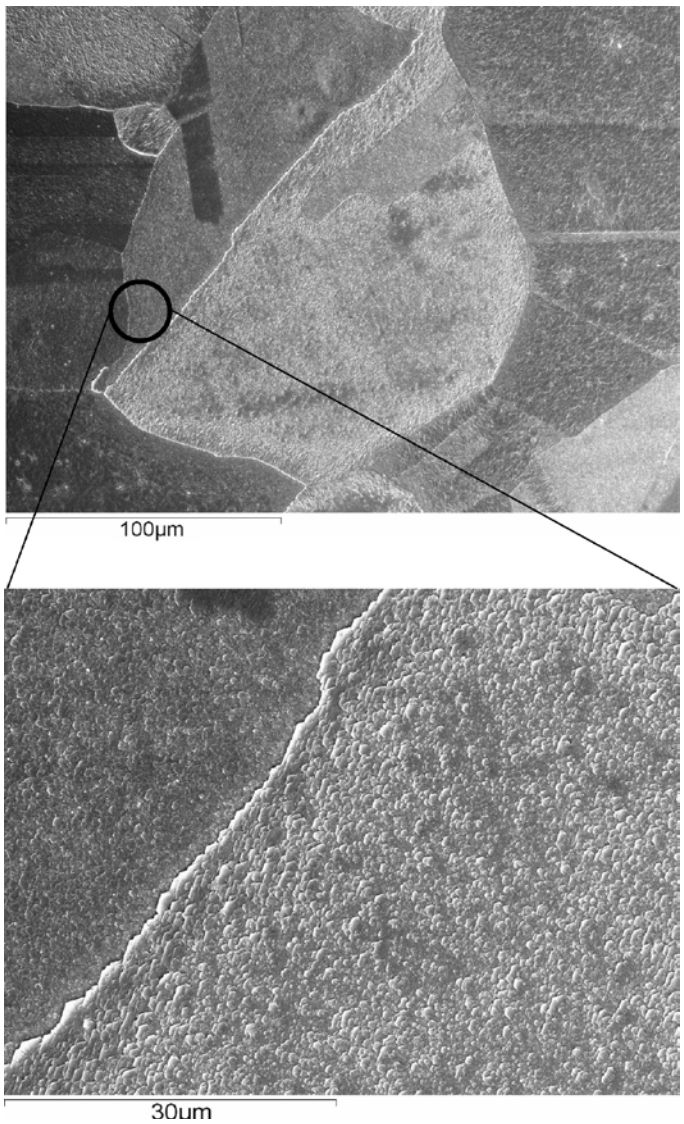

Figure 3-28 (continued). *As Figure 3-27, but with detailed characterization of individual areas. A complete set of such analyses is available – see Appendix B.*

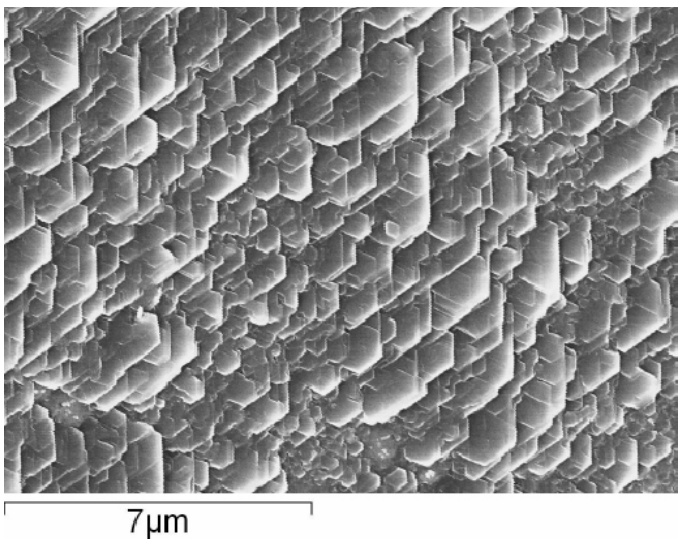

Figure 3-29. *Example of highly substrate-oriented Cu_2S growth, from part of region C in Figure 3-28.*

4 Conclusions

No SCC was found in SSRT testing of SKB copper tensile specimens at open-circuit potential in a range of NaCl solutions or synthetic sea water with addition of 5–50 mM Na_2S at room temperature or 80°C. Neither was there any SCC with small cathodic or anodic potentials applied, nor in a range of constant-strain test procedures.

The Cu_2S corrosion product was generally coarse, fragile, and easy to spall off in severe corrosion environments, e.g. high sulfide concentration, high temperature, and (although this was not definitely established) less perfect deaeration. But it could consist of very fine grains, relatively compact and adherent, when it was formed in a well-deaerated solution at room temperature. Generally, the film was found to have two layers: an inner, fine-grained layer and an outer, particulate layer.

There are many indications that the corrosion rate in such solutions can be controlled by inward diffusion of sulfide (HS^-) ions, but this is complicated by the additive effect of the hydrodynamic diffusion layer and the porous corrosion product film.

One can make the argument that if the corrosion rate is always controlled by inward sulfide diffusion, SCC and other kinds of localized corrosion should never occur.

However, the corrosion rate and sulfide film thickness were found to depend strongly on grain face orientation in electropolished specimens. There remains something of a contradiction between this finding (for which no particular orientation was most resistant, although (100) seemed statistically more so) and the idea that corrosion is mostly diffusion controlled in this system.

References

SKB's (Svensk Kärnbränslehantering AB) publications can be found at www.skb.se/publications.

Arilahti E, Lehtikuusi T, Saario T, Varis P, 2011a. Sulphide induced stress corrosion cracking of copper – Intermediate report 3. Research Report VTT-R-10541-10, VTT, Finland.

Arilahti E, Lehtikuusi T, Olin M, Saario T, Varis P, 2011b. Evidence for internal diffusion of sulphide from groundwater into grain boundaries ahead of crack tip in Cu OFP copper. Corrosion Engineering, Science and Technology 46, 134–137.

Arilahti E, Mattila M, Lehtikuusi T, Saario T, Varis P, 2012. Sulphide-induced embrittlement of CuOFP – Intermediate Report 2. Research Report VTT-R-00291-12, VTT, Finland.

Newman R C, Rumash K, Webster B J, 1992. The effect of pre-corrosion on the corrosion rate of steel in neutral solutions containing sulphide: relevance to microbially influenced corrosion. Corrosion Science 33, 1877–1884.

Rickard D, Luther G W, 2006. Metal sulfide complexes and clusters. Reviews in Mineralogy and Geochemistry 61, 421–504.

Smith J M, 2007. The corrosion and electrochemistry of copper in aqueous, anoxic sulphide solutions. PhD thesis. University of Western Ontario, Canada.

Smith J, Qin Z, King F, Werme L, Shoesmith D W, 2007. Sulfide film formation on copper under electrochemical and natural corrosion conditions. Corrosion 63, 135–144.

Sun W, Nešić S, Young D, Woollam R C, 2008. Equilibrium expressions related to the solubility of the sour corrosion product mackinawite. Industrial & Engineering Chemistry Research 47, 1738–1742.

Taniguchi N, Kawasaki M, 2008. Influence of sulfide concentration on the corrosion behaviour of pure copper in synthetic seawater. Journal of Nuclear Materials 379, 154–161.

Tossell J A, 2000. Metal–thiometalate transport of biologically active trace elements in sulfidic environments. 2. Theoretical evidence for copper thioarsenite complexing. Environmental Science & Technology 34, 1483–1488.

Description of appendices

Appendix A describes additional work carried out to explore the possibility that the presence of thiosulfate from inadvertent air exposure could have caused more severe intergranular damage than was observed in well-deoxygenated sulfide solutions.

Appendix B gathers all the EBSD data.

Appendix A

Grain boundary phenomena observed in flat samples and slow strain rate test samples

Polished cross-sections were made of copper samples that had been exposed to a range of conditions shown in Table A-1, below. In part this was to test the idea that inadvertent air exposure may have produced thiosulfate, by sulfide oxidation, in work carried out elsewhere (Arilahti et al. 2012). Some potentials reported by the VTT authors in their two reports were too positive to be attributed to a fully reduced sulfide environment.

Table A-1. Conditions of exposure of additional samples studied after learning of recent Finnish work.

Sample ID	T, °C	Testing Environment (exposure or SSRT)	Final pH	Notes
Unstressed samples made of SKB copper from UWO (batch I)				
Flat_A	RT	0.414 M NaCl+3.12 mM Na_2S *[Total of 100 ppm "S"]*	11.08*	5 days
Flat_B	RT	0.414 M NaCl+1.56 mM Na_2S+0.78 mM $Na_2S_2O_3$ *[Total of 100 ppm "S"]*	11.44*	5 days
Flat_C	RT	0.414 M NaCl+1.56 mM $Na_2S_2O_3$ *[Total of 100 ppm "S"]*	11.26*	5 days
Samples after SSRT tests, cross-section along gauge length; Tensile specimens – from SKB				
SSRT-I	RT	0.414 M NaCl+1.56mM Na_2S+0.78mM $Na_2S_2O_3$ *[Total of 100 ppm "S"]*	11.11*	Solution not refreshed
SSRT-II	RT	0.414 M NaCl+3.12 mM Na_2S+1.56 mM $Na_2S_2O_3$ *[Total of 200 ppm "S"]*		Solution refreshed once in 2 days
SSRT-IV	RT	Air	n/a	to fracture
SSRT-V; *[–20 mV vs. Cu]*	RT	Artificial sea salt + 10 mM Na_2S	9.04	to fracture

* *pH adjusted using NaOH solution.*

Nothing remarkable was observed in any of the flat samples, and no evidence for cracking was observed, but for some time it was thought that there was evidence for a bizarre intergranular phenomenon in sample SSRT-1, whose conditions of exposure are defined in Table A-1. Figure A-1 shows what appears to be a granular network on the polished (unetched) cross-sectional surface of this sample. However further examination did not support the notion that this was some kind of deep, penetrating corrosion that had occurred during exposure to the sulfide-thiosulfate solution. Not least, this was because the grain size of the material was much smaller than that of the apparent granular network (Figure A-2).

Informal optical microscopy of the polished cross-section of sample SSRT-1 showed that there were particles in the microstructure that were reacting rapidly with laboratory air and giving the appearance of a granular network. No detailed analysis was done, but we speculate that these are copper phosphides that react with laboratory air to give phosphoric acid, which corrodes and discolours an area around each particle. Probably the particles predominate along prior grain boundaries of the structure, which explains why the surface has a coarse granular appearance.

An unanswered question relates to the possible relevance of phosphorus to the intergranular corrosion phenomena reported by others (Arilahti et al. 2012). In any event, we have not reproduced such phenomena, although we note that evidence for deep penetrating intergranular corrosion was only observed when the grain boundaries were opened up by fatigue, not when they were subject to simple tensile overload. This observation was reported too late to be of use in our main study.

Figure A-1. *Apparent granular network on the polished, unetched surface of sample SSRT-I described in Table A-1. The gauge diameter was 3 mm.*

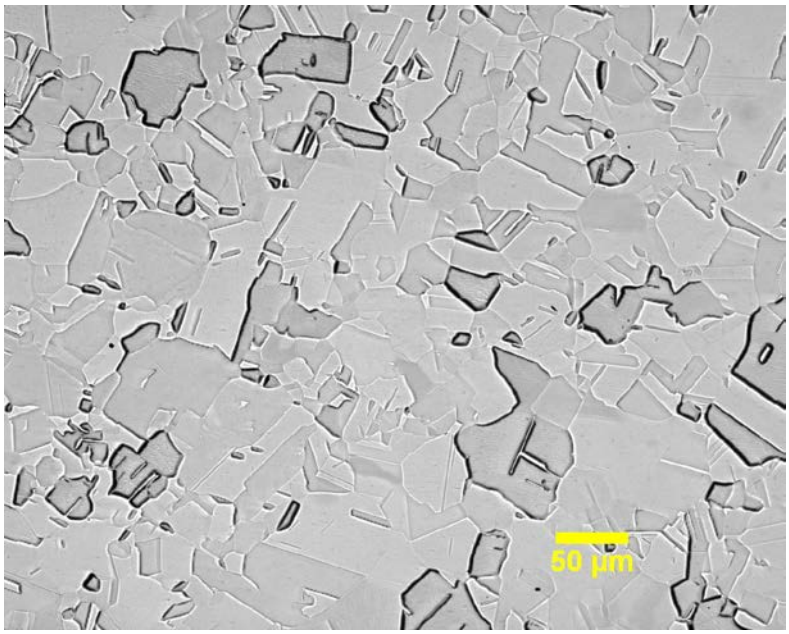

Figure A-2. *The actual microstructure of the copper used for test SSRT-1, showing a grain size much smaller than the apparent granular network in Figure A-1 (polished at Buehler using vibratory polisher and ammonium perchlorate etch).*

Appendix B

EBSD data

Table B-1. Sample preparation and exposure conditions for samples analyzed by EBSD.

Specimen	Sample preparation				Exposure after EBSD
	Before EBSD		After EBSD*		
	Mechanical polishing	Electropolish in 10 M H_3PO_4 at 2 V	Mechanical polishing	Electropolish in 10 M H_3PO_4 at 2 V	
1	3 µm	5 min	Mildly with 0.05 µm	60 s	Synthetic seawater + 2 mM Na_2S for 48 h
2	0.05 µm		–		
3	3 µm		–		
4	0.05 µm		–		

* To remove carbon impurities accumulated on the surface from the EBSD analysis.

All figures are given in the same manner in Appendix B, in three parts. Some figures are given on two pages because of the size.

Part 1: Inverse pole figure map showing the orientation of the different grains.

Part 2: SEM micrograph with orientation mentioned for the grains on which film morphology was imaged.

Part 3: SEM images showing the different morphology of the sulfide film on different grains.

Specimen 1 – Region 1

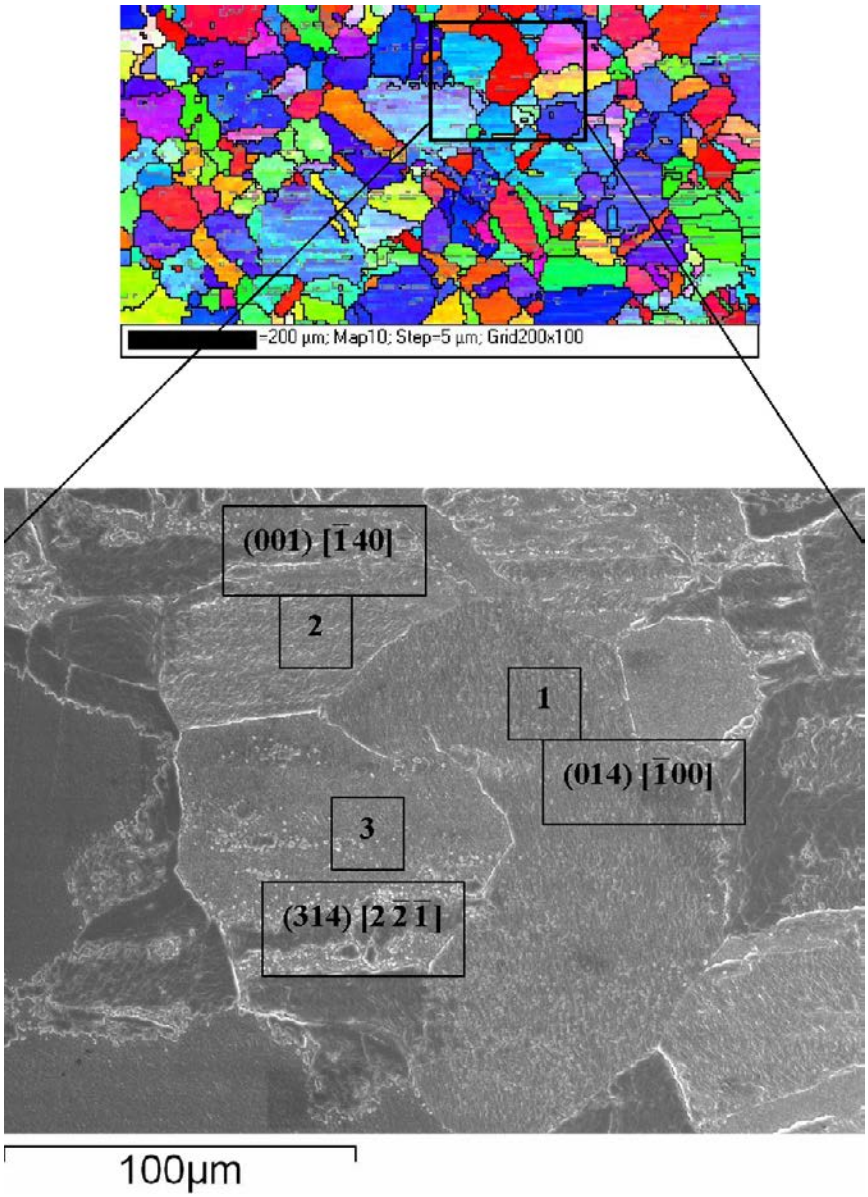

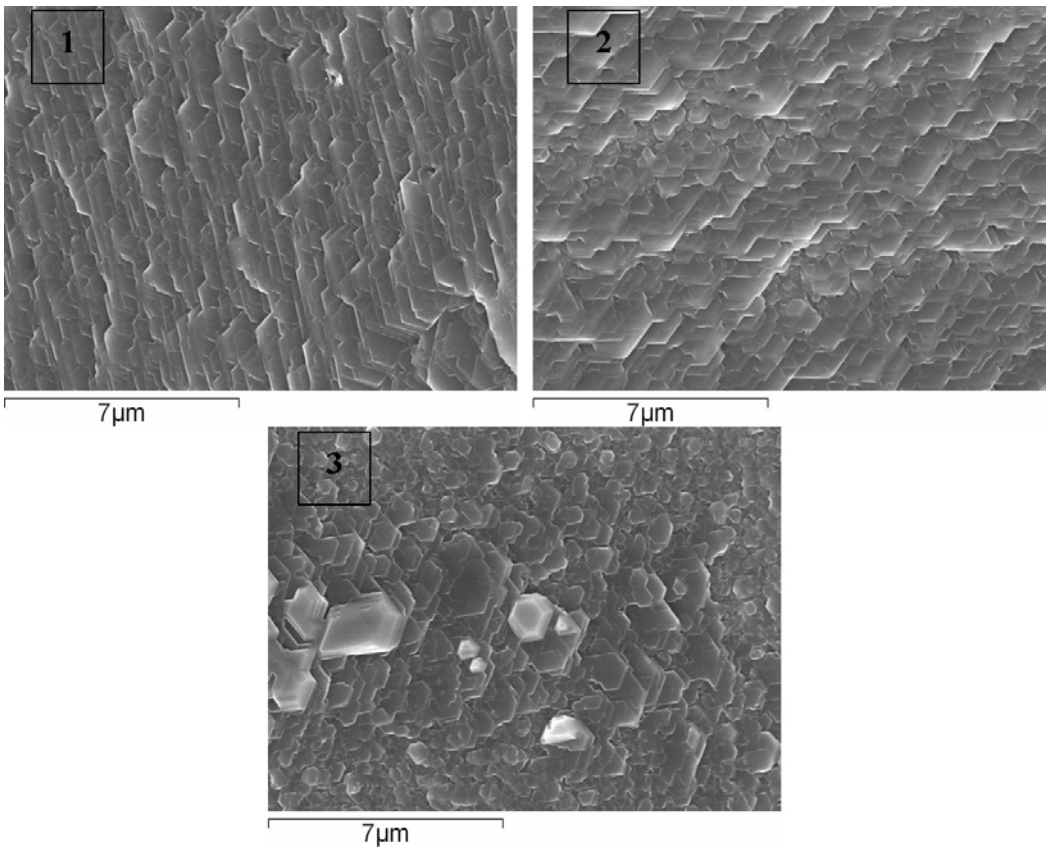
1
7µm
2
7µm
3
7µm

Specimen 1 – Region 2

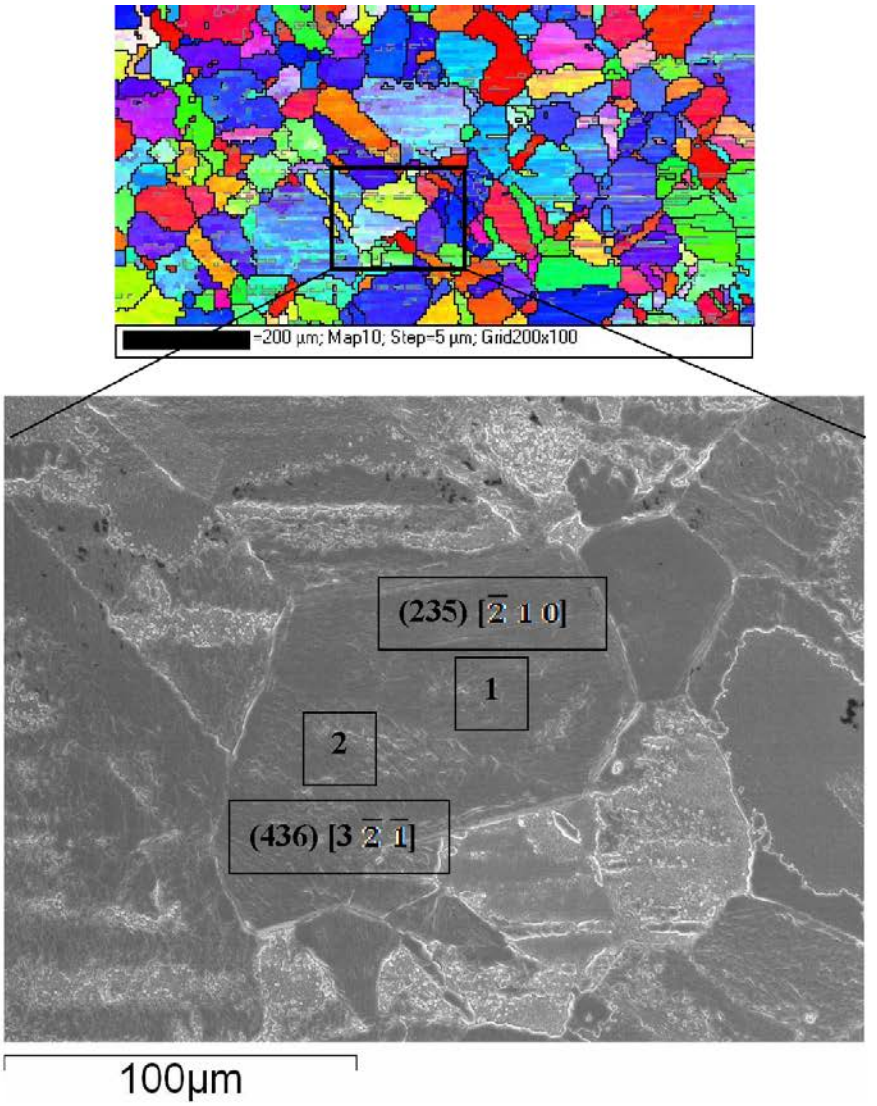

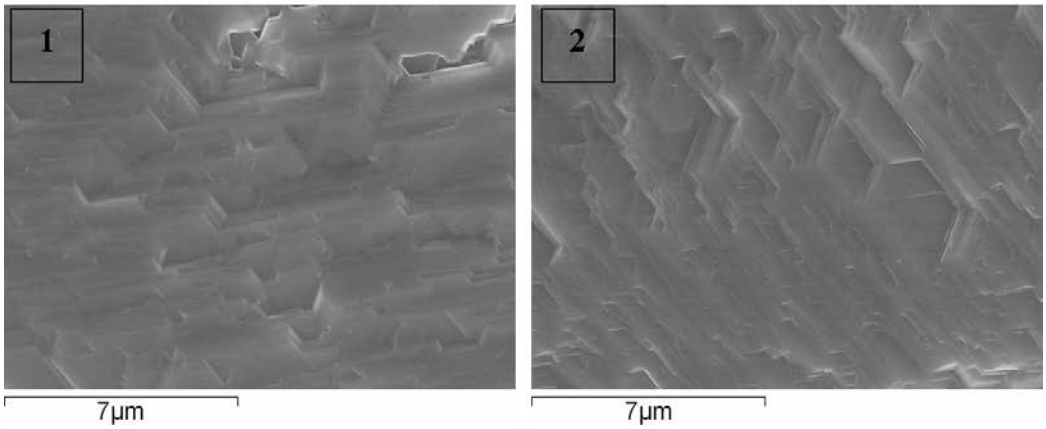

Specimen 1 – Region 3

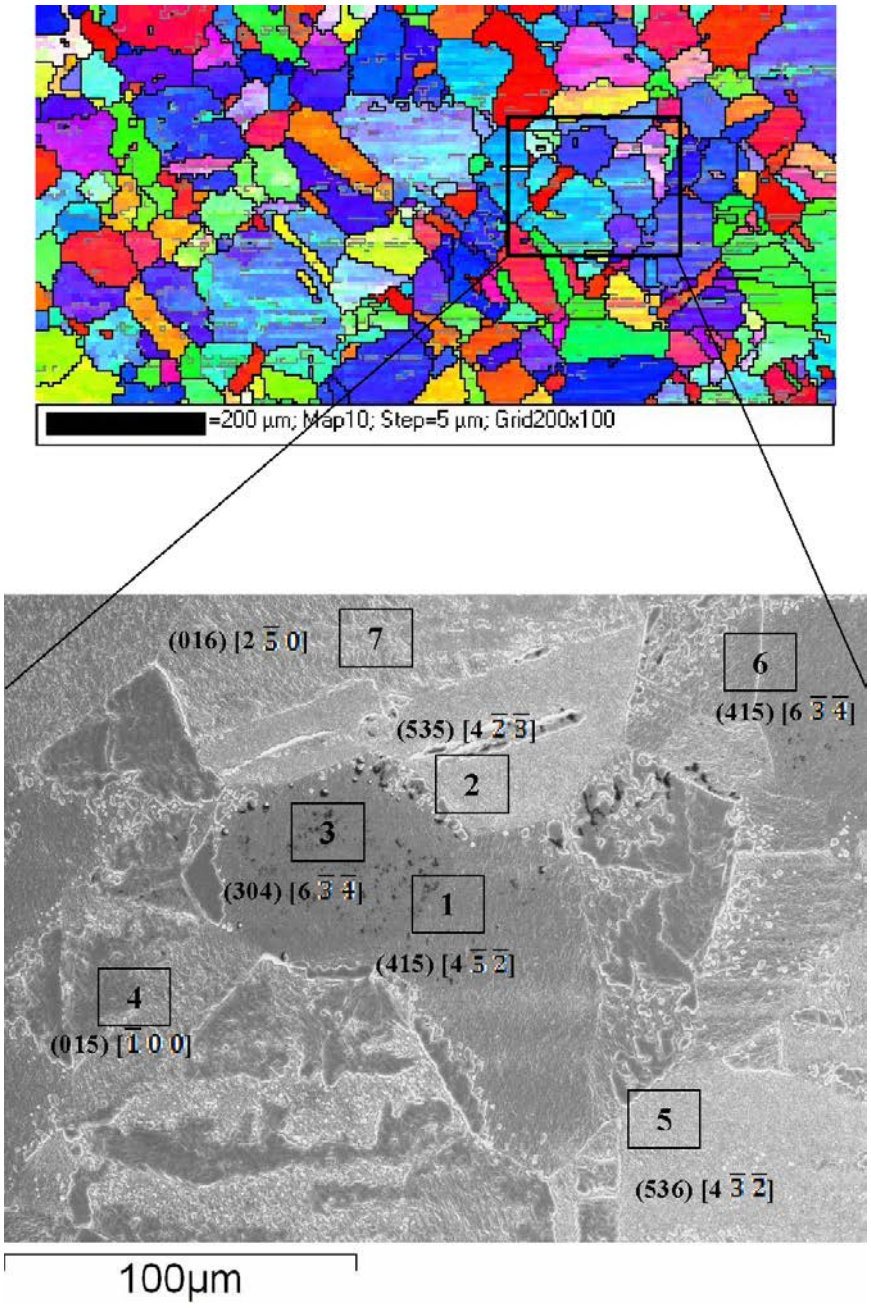

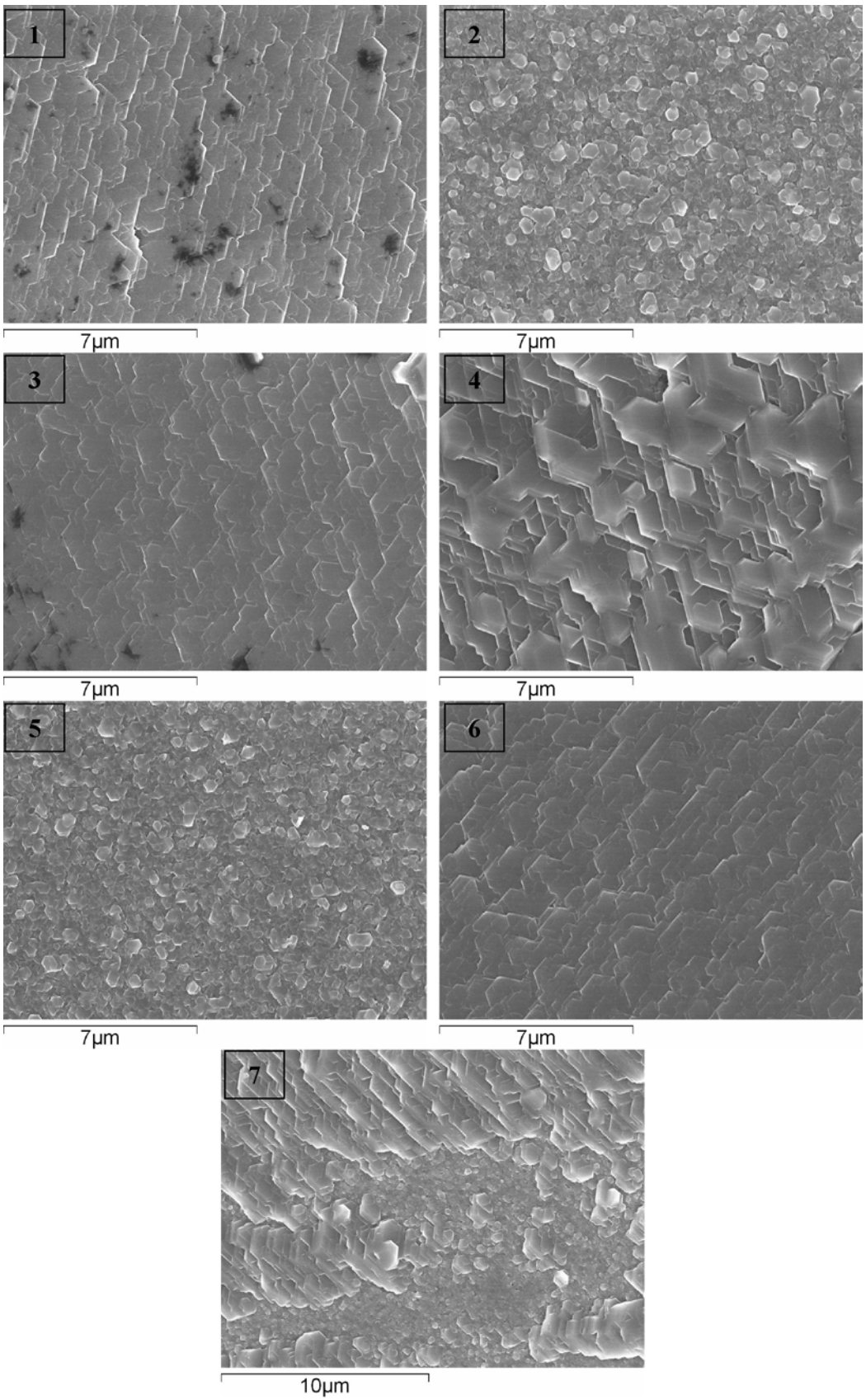
1
7µm
2
7µm
3
7µm
4
7µm
5
7µm
6
7µm
7
10µm

Specimen 2 – Region 1

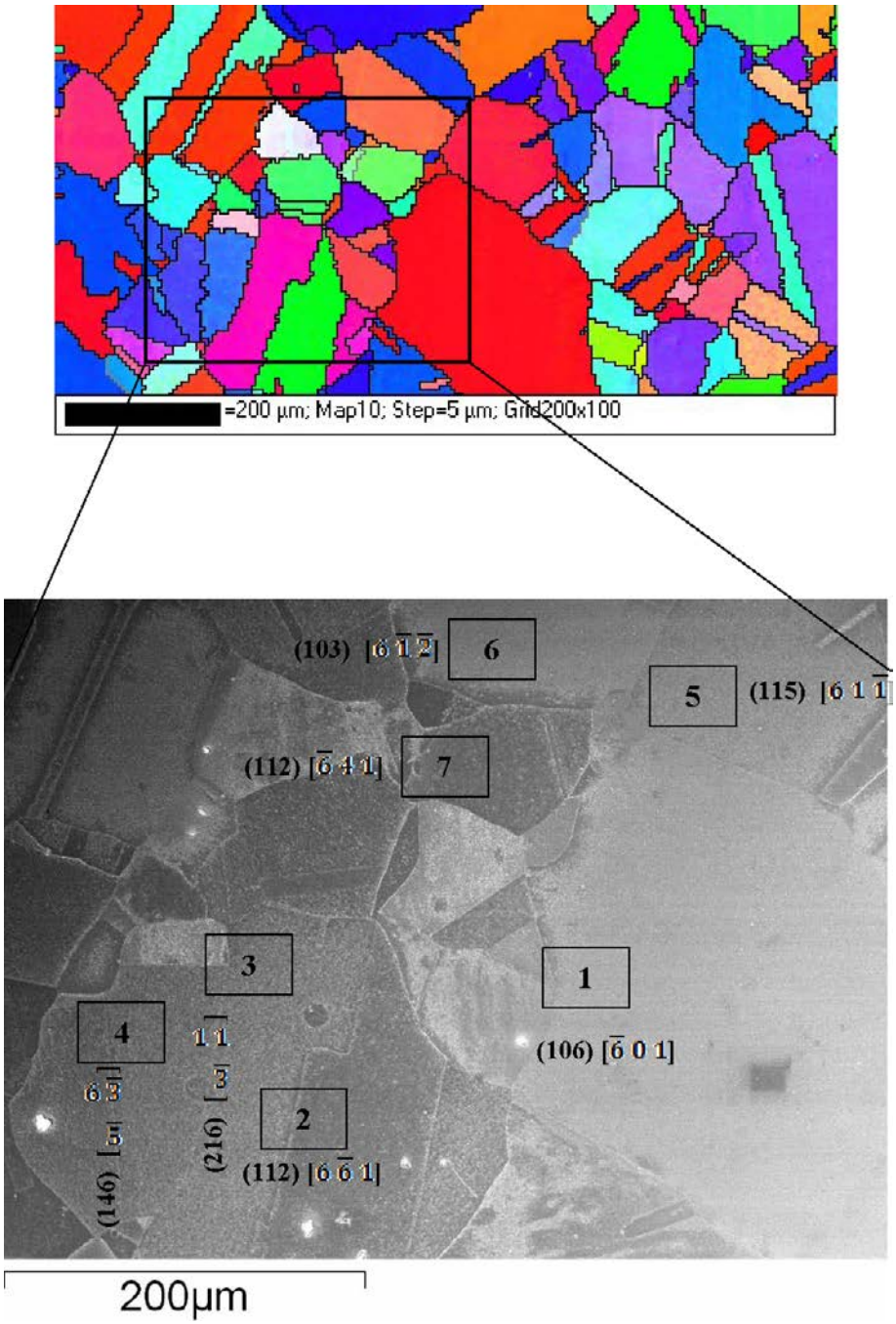

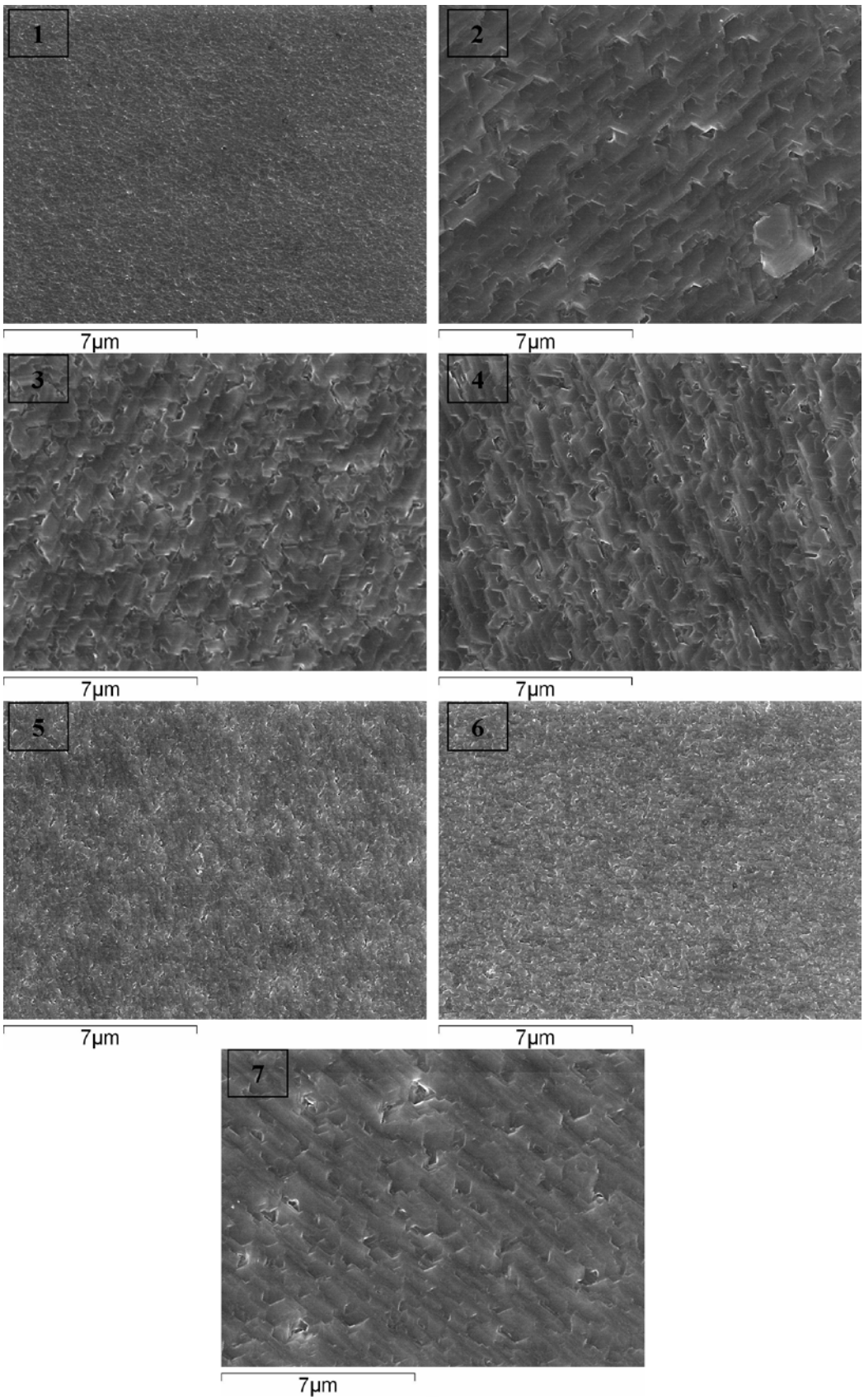
1
7µm
2
7µm
3
7µm
4
7µm
5
7µm
6
7µm
7
7µm

Specimen 2 – Region 2

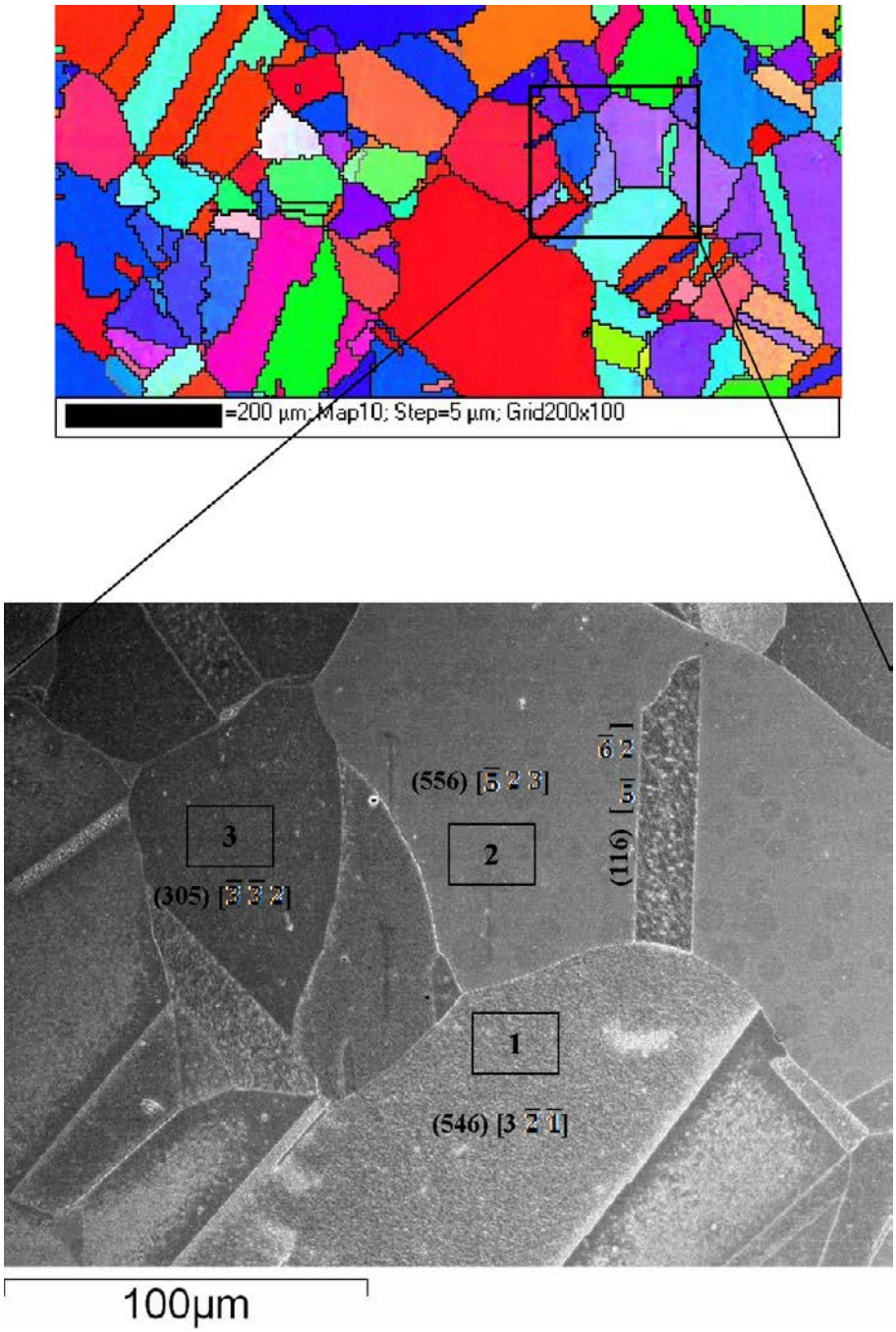

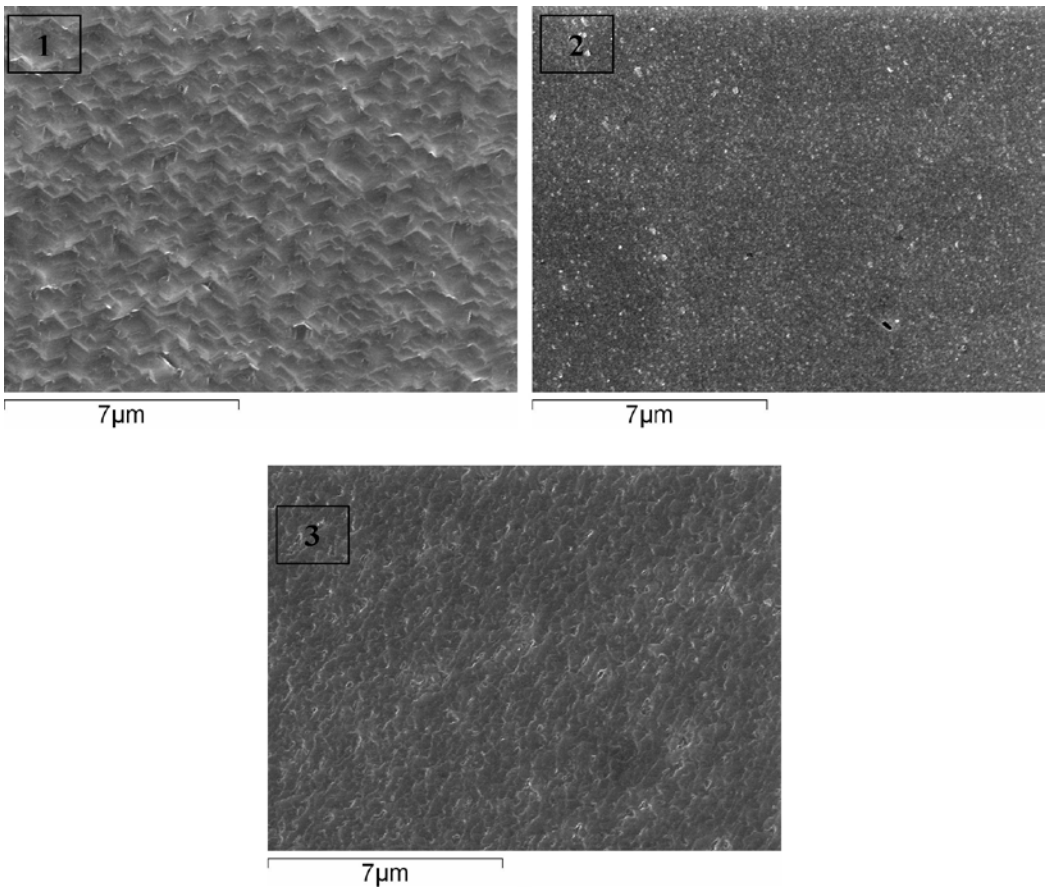
1
7µm
2
7µm
3
7µm

Specimen 3 – Region 1

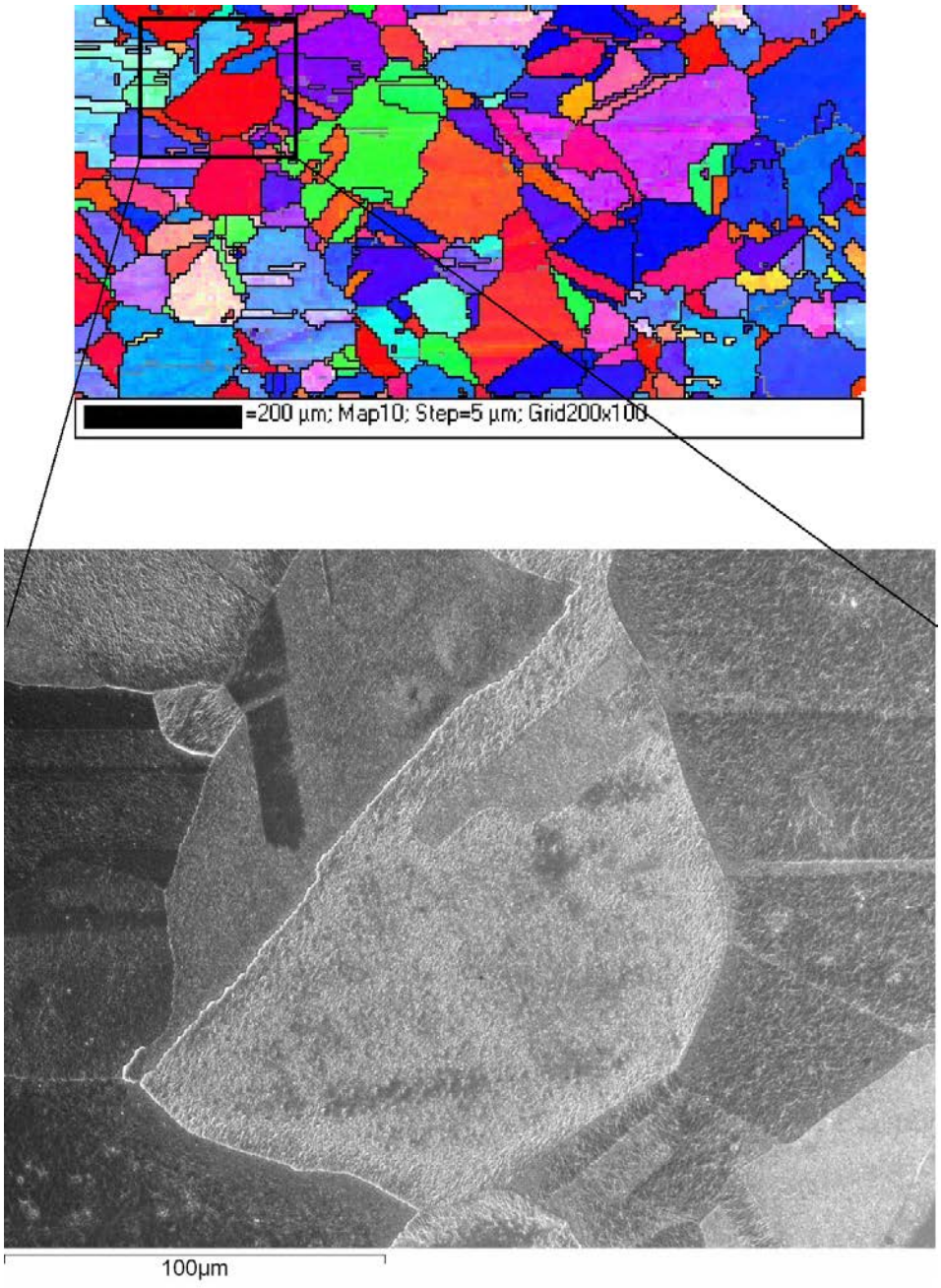

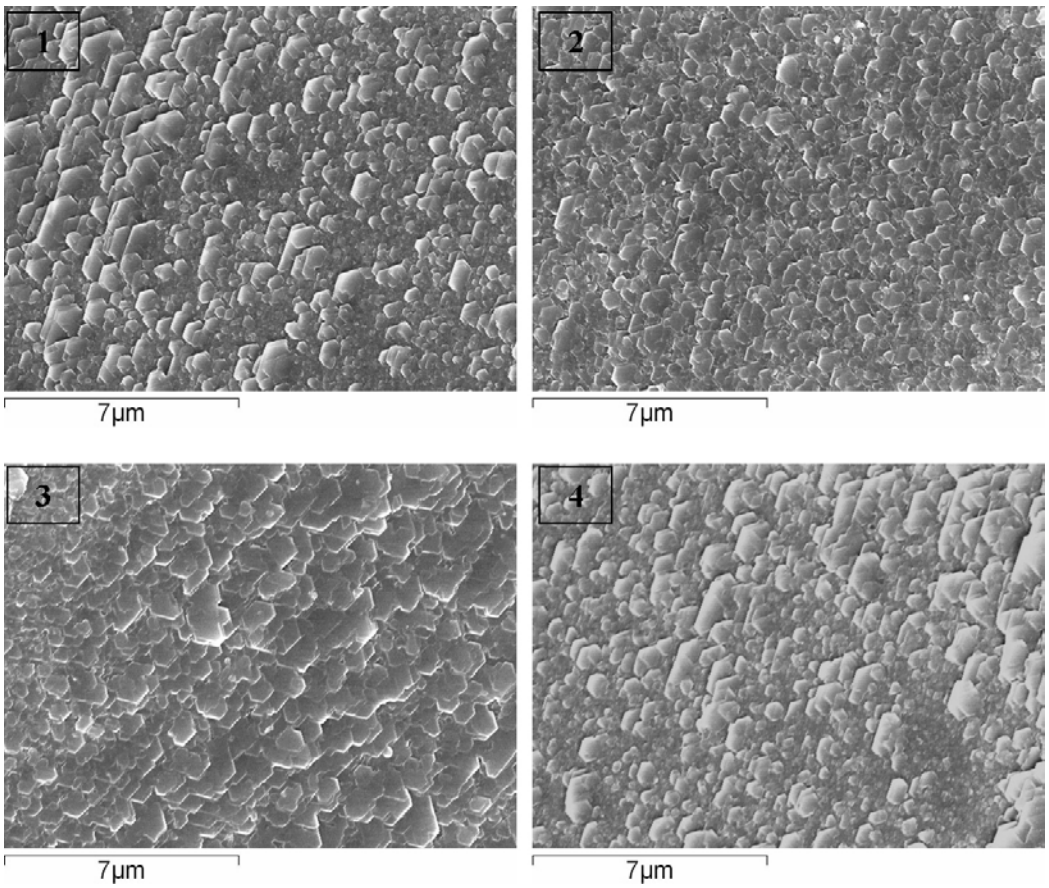
1
7µm
2
7µm
3
7µm
4
7µm

Specimen 3 – Region 2

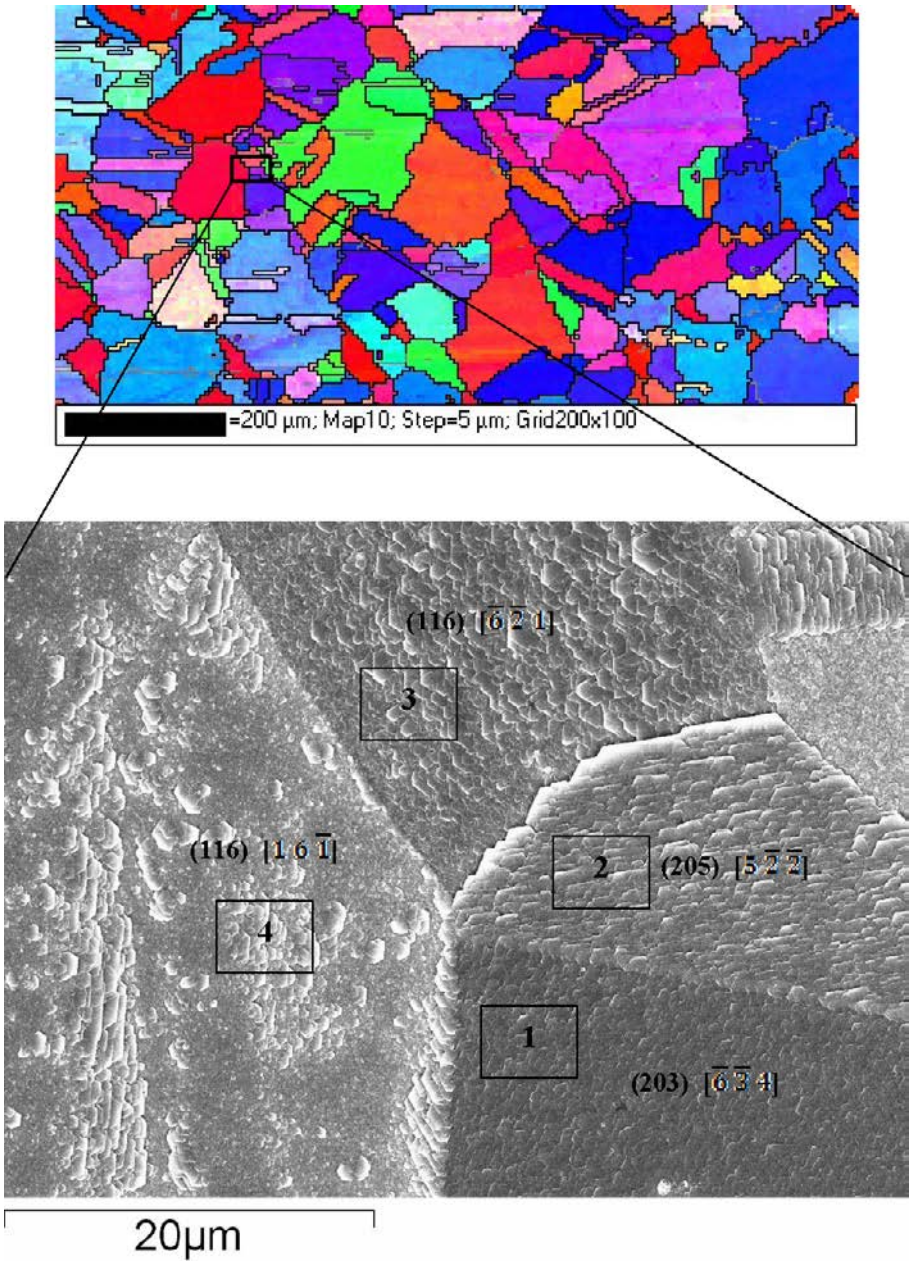

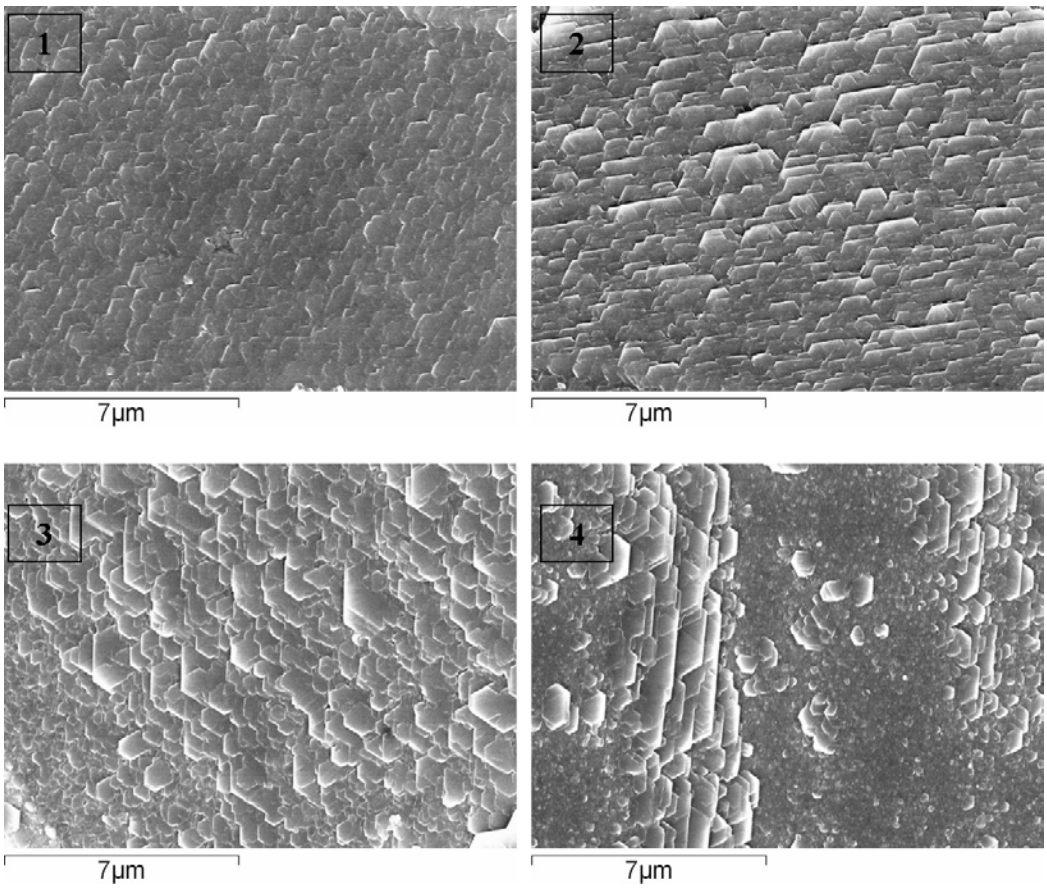
1
7µm
2
7µm
3
7µm
4
7µm

Specimen 3 – Region 3

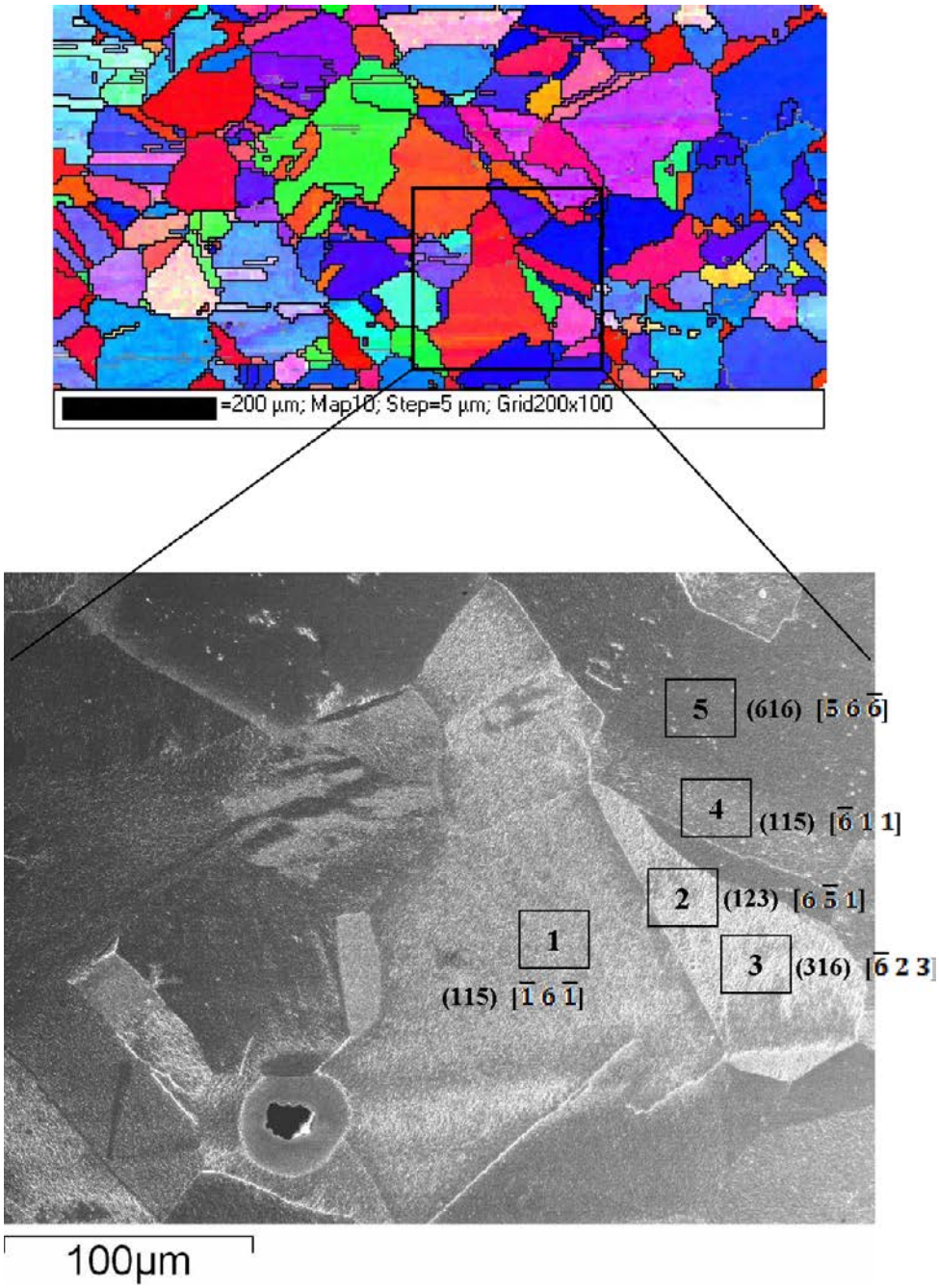

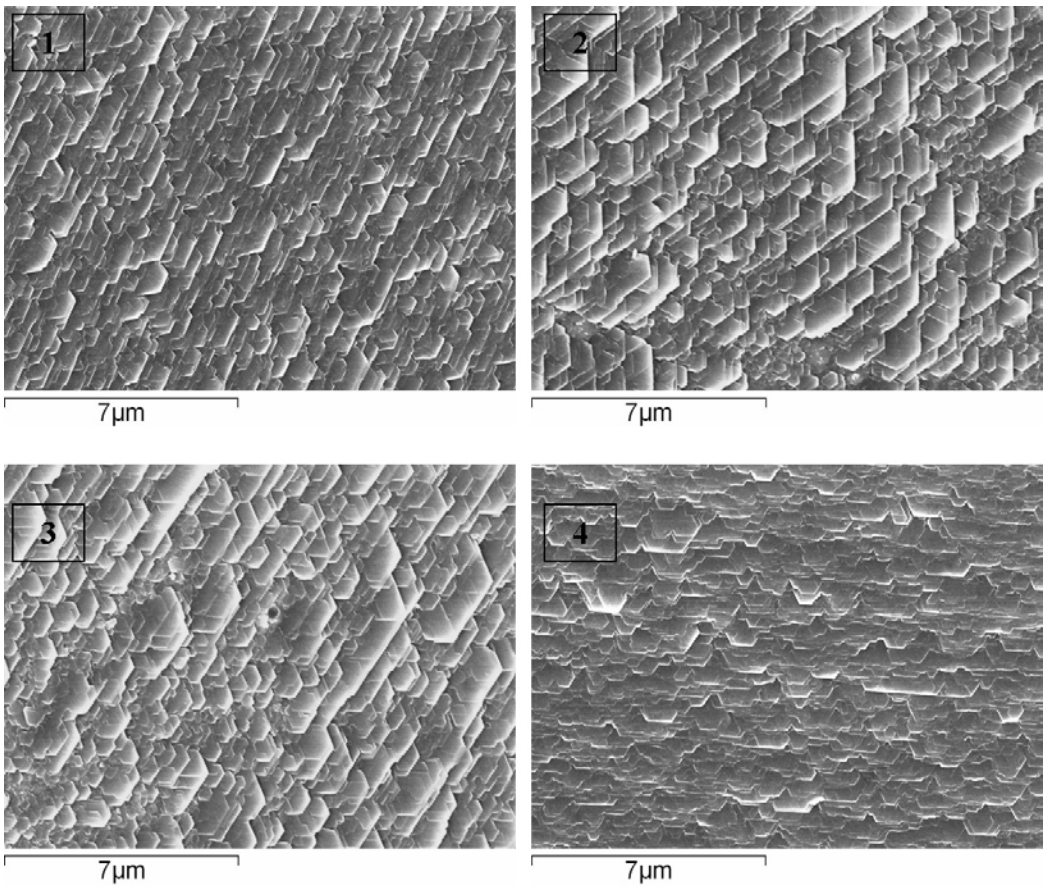
1
7µm
2
7µm
3
7µm
4
7µm
5
7µm

Specimen 3 – Region 4

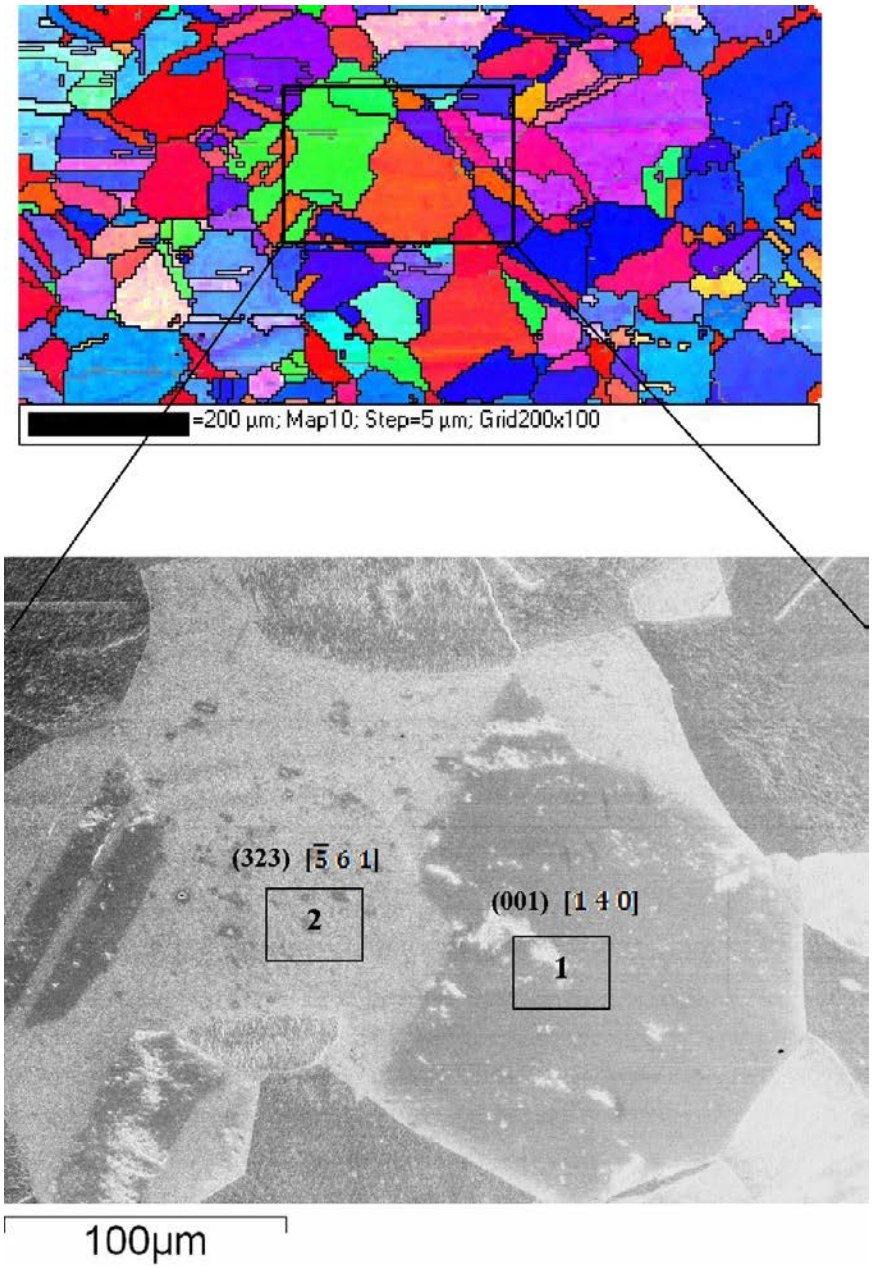

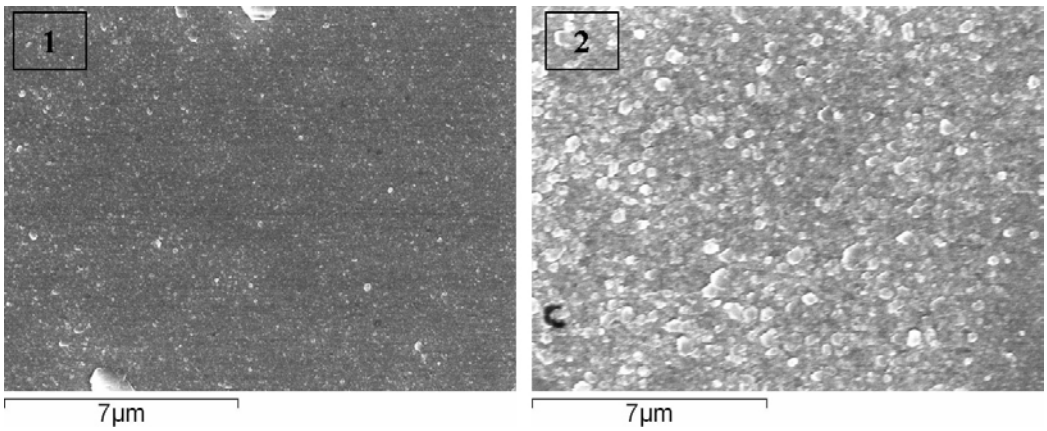

Specimen 4 – Region 1

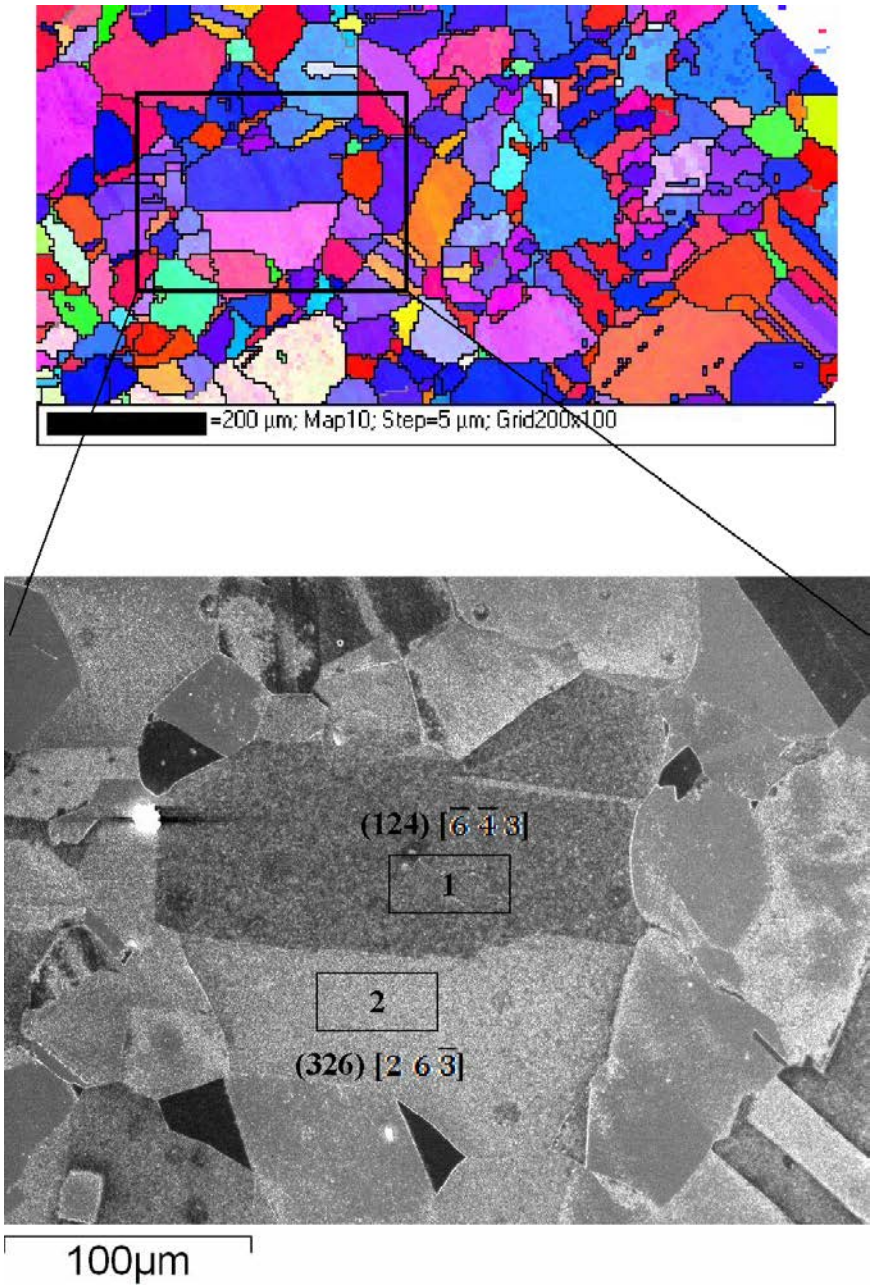

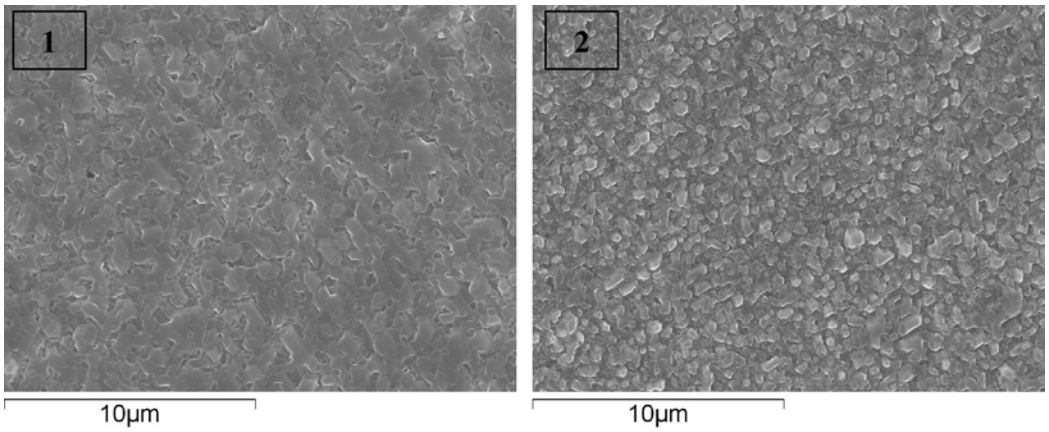

Specimen 4 – Region 2

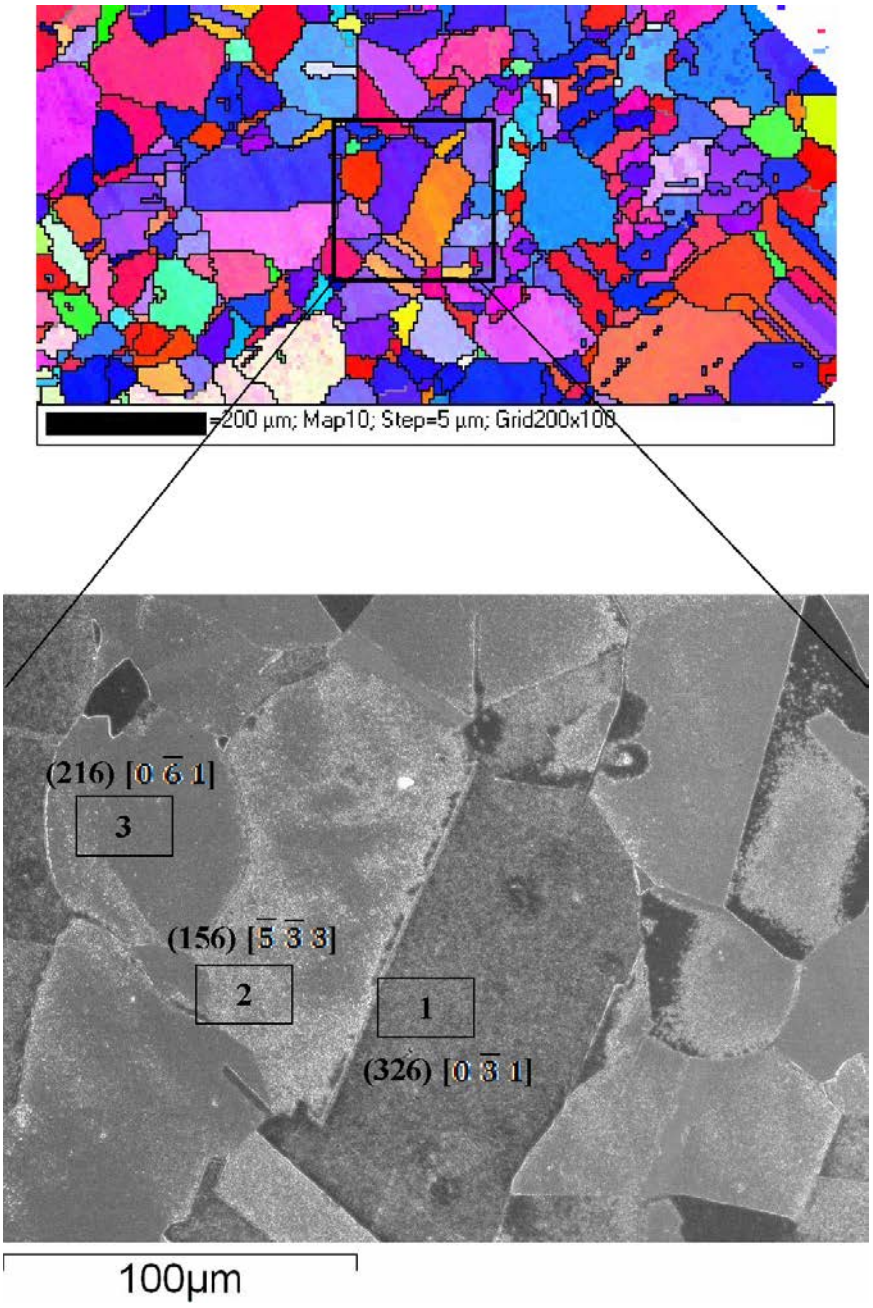

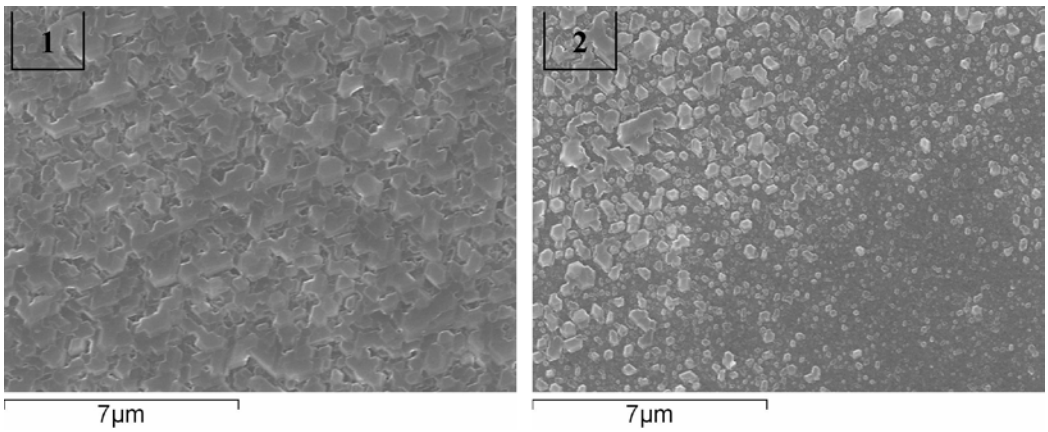
1
7µm
2
7µm

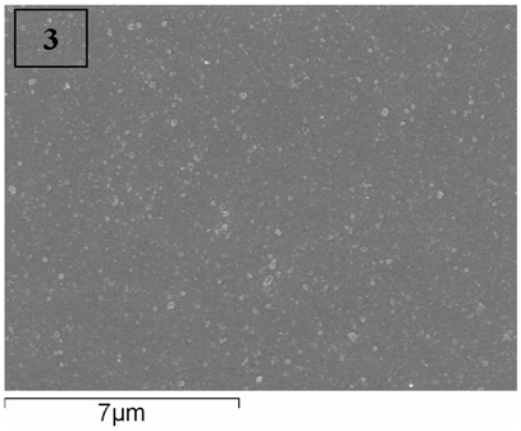
3
7µm

Specimen 4 – Region 3

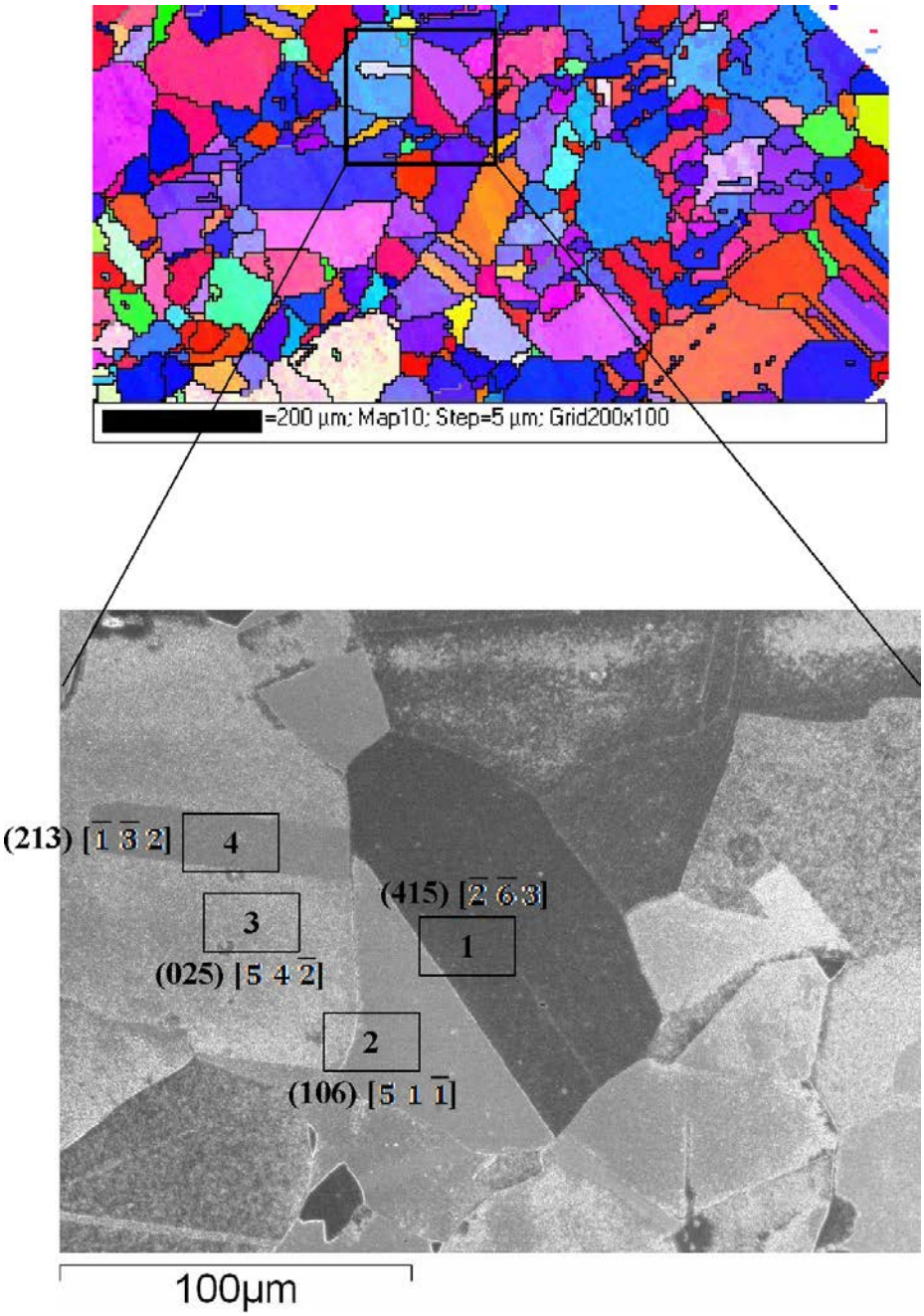

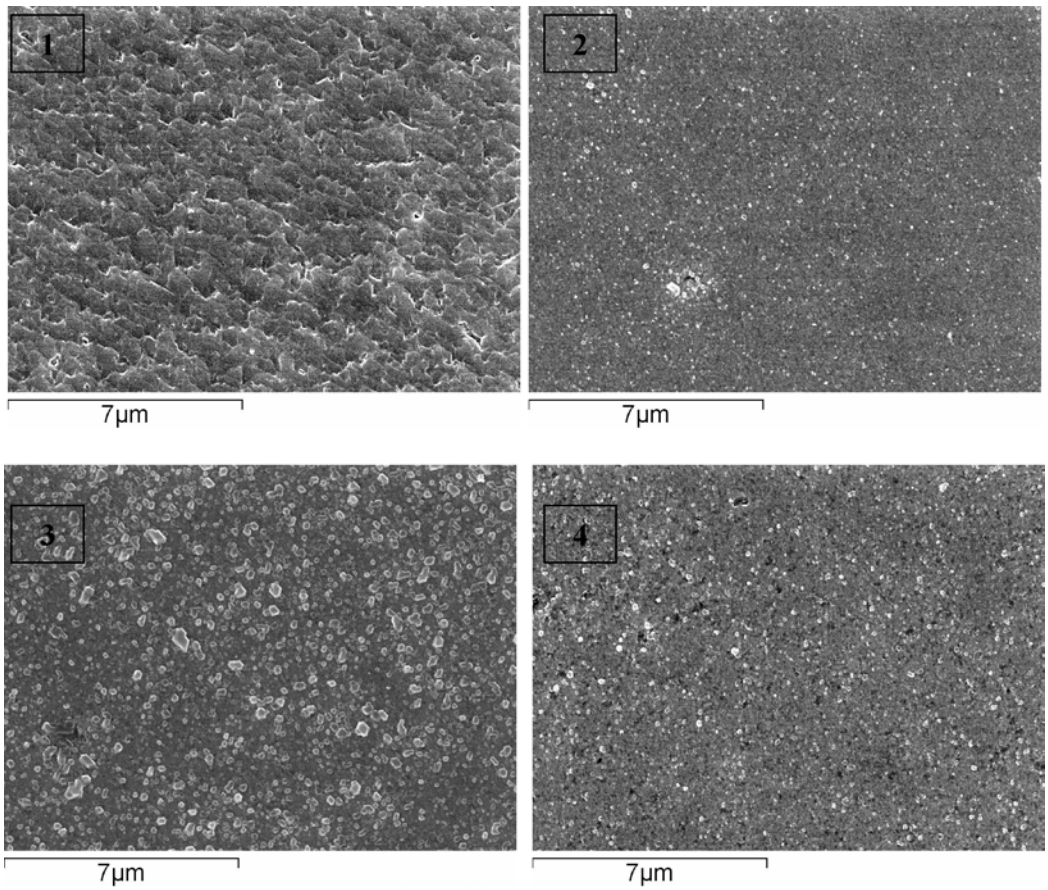
1
7µm
2
7µm
3
7µm
4
7µm